Memoirs of the Faculty of Engineering, Nagoya University
Vol. 27, No. 1. (1975)

STICK-SLIP MOTION AND CHARACTERISTICS OF FRICTION IN MACHINE TOOL SLIDEWAY

SHINOBU KATO, KATSUMI YAMAGUCHI
Department of Mechanical Engineering

TSUNEO MATSUBAYASHI
Suzuka College of Technology

NORIO SATO
Toyota Motor Co. Ltd.

(Received May 27, 1975)

CONTENTS

1. Introduction

Dynamic behaviour of a tool or a work which moves along a machine tool slideway is considered to be one of the most important factors that have a great influence on the machining accuracy. In a finishing process of machining, unstable behaviour of the moving element, that is stick-slip motion, occurs owing to the low driving speed of the element, and this unstable behaviour leads to a deterioration of the machining accuracy.

Many papers on the stick-slip motion have been presented by Bowden[1], Rabinowicz[2], Sampson[3], Matsuzaki[4], Brockley[5] and Singh[6], et al. Most of them, however, have treated the unstable behaviour of the moving element from the view point of lubrication or vibration mechanics. In order to clarify the relation between the stick-slip motion and the frictional characteristics of the machine tool slideway from a practical point of view, more investigations are desired.

In this research, the dynamic behaviour of a moving element of an actual machine tool slideway is examined under various sliding conditions, that is a variety of vibrational properties of the driving system and properties of applied lubricant. Then, the fundamental characteristics of the stick-slip motion are clarified experimentally. Basing on these experimental results, a mechanism of the stick-slip motion is revealed, the boundary condition for occurrence of the stick-slip motion is clarified, and the relation between properties of the stick-slip motion and frictional characteristics is examined quantitatively.

The behaviour of the stick-slip motion depends strongly on both characteristics of static friction during the stick period and kinetic friction during slip period. Especially the stick-slip motion is intimately associated with static friction as described later. When two surfaces are in stationary contact under boundary lubrication, the static frictional force gradually changes with increase of contact time or stick period.

This paper presents experimental results on the fundamental characteristics of stick-slip motion. Based on the results, the time-dependence of static friction is clarified, and the mechanism of the time-dependence of static friction is investigated theoretically. Then, the influence of lubricants and surface topography on the characteristics of static friction is discussed experimentally and theoretically, and to estimate the surface topography in the view point of the frictional characteristics a non-dimensional numerical parameter so-called the coefficient of surface topography is proposed.

2. Characteristics of Stick-Slip Motion

2. 1. Experimental

The slideway used in this experiment is composed of inverted V and flat shape surfaces as shown in Fig. 1, which are generally used in the actual machine tool. The slideway G and the slider S are both made of cast iron, and the surfaces are finished by scraping.

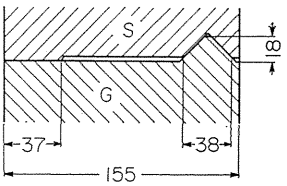

Fig. 1. Cross section of slideway.

Experimental apparatus is illustrated in Fig. 2 schemetically. For a basic study of the sliding behaviour of the slider S, a driving system is introduced, so that its mechanical

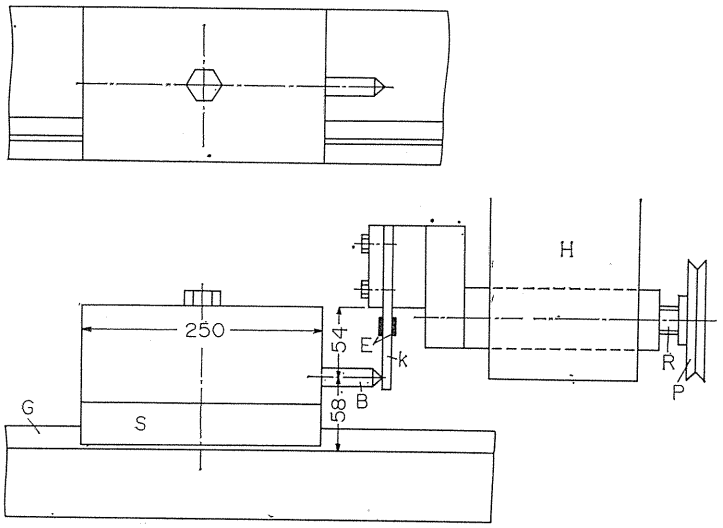

Fig. 2. Experimental apparatus.

properties can be estimated clearly and accurately. The slider S is driven by pushing at a projection B of the slider through a straight leaf spring k (stiffness of which is k) which is attached to an accurate screw mechanism. The stiffness of the driving system can be varied by changing the dimensions of the leaf spring k. Mass of the slider is varied by changing a dead weight which rests on the slider S. Surfaces of the slideway and slider are spread with lubricant thoroughly. A few passes of run-in sliding are made in advance of experiment so that excess lubricant may be removed from the surfaces and the experiment conducted under stable conditions. Experimental conditions are shown in Table 1, and the four kinds of lubricant used herein are shown in Table 2.

Dynamic behaviour of the slider in the sliding direction is measured by a strain gauge E which detects the deflection of the spring, and it is recorded by an electromagnetic oscillograph.

Table 1. Experimental conditions

Weight of slider	kg	$W_1=11.3$	$W_2=36.0$	$W_3=53.2$
Apparent contact area	cm^2		$A=167.5$	
Contact pressure	kg/cm^2	$w_1=0.067$	$w_2=0.215$	$w_3=0.318$
Stiffnesses of driving system	kg/mm	$k_1=27.3$	$k_2=86.9$	$k_3=128.5$
Driving speed	mm/min		$v=0.0022\sim92$	

Table 2. Lubricants

Lubricants	Viscosity cSt at 20°C	Remarks
A	195.4	Naphthene base mineral oil
B	214.0	Commercial slideway lubricant
C	1010.5	Non-drying vegetable oil
D	62.8	Animal oil

Relation between applied load and deflection of the springs used in this experiment is shown in Fig. 3. It is seen in the figure that each of these springs has good linearity in the range of the experiment. Experimental records of free vibration of these springs are shown in Fig. 4. The natural frequencies of these springs are greater than 800 Hz and they are so high compared with the frequency of the stick-slip motion that the springs can follow the motion of the slider and the dynamic behaviour of the slider can be investigated exactly.

Figure 5. shows the vibratory system of this experimental apparatus which con-

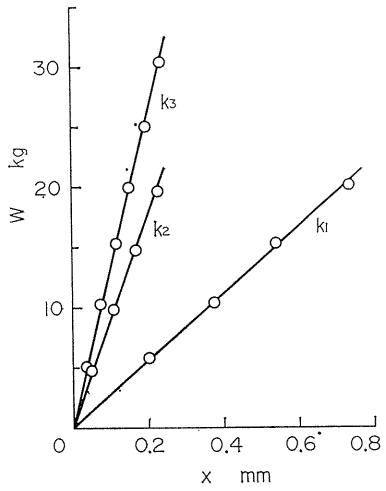

Fig. 3. Relation between applied load and deflection of springs

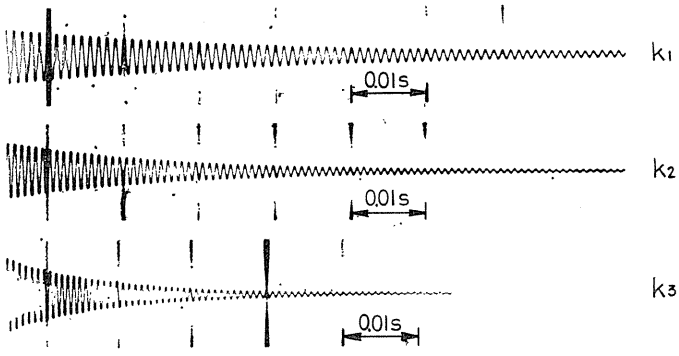

Fig. 4. Free vibration of driving springs

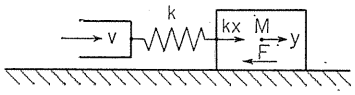

Fig. 5. Diagram of vibratory system.

sists of the slider and the driving mechanism. The figure indicates driving speed v, spring constant k of the driving mechanism, deflection x of the spring, displacement y of the slider M, and frictional force F acting on the slider.

Figure 6 illustrates the stick-slip motion. In the figure, (a), (b), (c) and (d) indicate deflection x of the spring, displacement of the driving point, displacement y of the slider, and sliding speed $\dot{y}$ of the slider, respectively. In the curve (a),

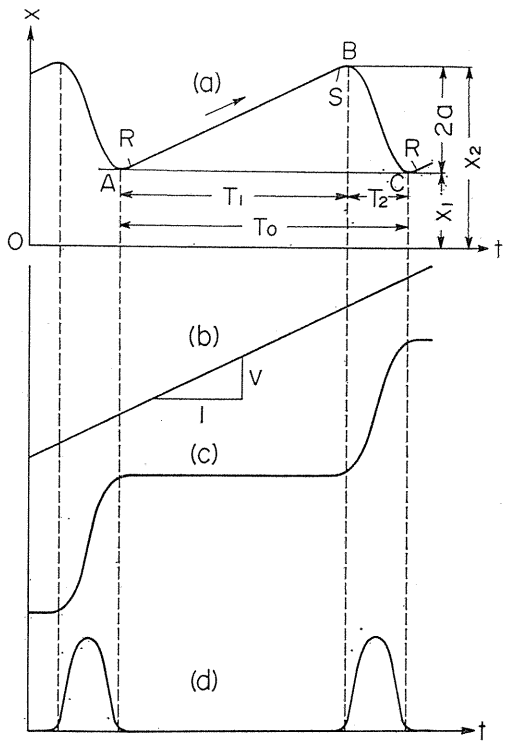

Fig. 6. Stick-slip motion

one cycle of the stick-slip motion is represented by ABC. AB is the stick period (T_1 is the stick time) during which the slider M rests on the slideway as seen in the curve (c). Hence the sliding speed $\dot{y}=0$ as shown in the curve (d) and in this period $F=kx$. BC is the slip period (T_2 is the slip time) during which the slider slides along the slideway as shown in the curve (c). In this period $\dot{y}\geq v$, and at the first half of the slip period $F\leq kx$ and at the later half $F>kx$. Strictly speaking, at the point S just before the point B the slider begins to slip gradually; at the point B $\dot{y}=v$, at the point C $\dot{y}=v$ again, and at the point R just after the point C the slider rests and $\dot{y}=0$. Consequently, in this meaning, RS is the stick period, and SR is the slip period.

2. 2. Characteristics of Stick-Slip motion

Experiments are conducted under various conditions, that is, variety of applied lubricant, stiffness of driving system, weight of slider.

Figure 7 shows an example of experimental records of the stick-slip motion at

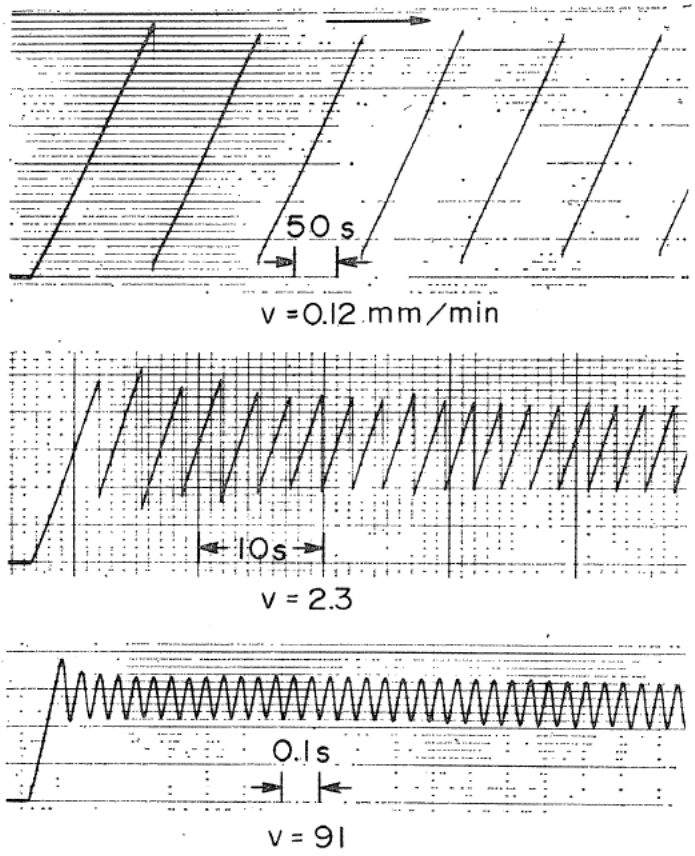

Lubricant *A*, k=86.9kg/mm, W=36.0kg

Fig. 7. Experimental records of stick-slip motion.

different driving speeds. The figure indicates a typical stick-slip motion and the nature of the motion is seen to vary with the driving speed.

Figure 8 illustrates variation of the stick-slip amplitude a with increase of the driving speed. In the figure, the amplitude a is presented in the non-dimensional form ak/W, where k is stiffness of the driving system and W is weight of the slider. It is seen in the figure that the amplitude a decreases as the driving speed v increases; but the magnitude of a and its decreasing tendency with v vary markedly by the kind of the applied lubricant. That is, in the care of lubricant *A*, the applitude is held nearly constant below the speed at point A_1 as shown in Fig. 8, and at the speed between A_1 and A_2 the amplitude decreases abruptly. In the case of the lubricants *B*, *C* and *D*, there is a tendency that the magnitude of a is considerably smaller than in the case of lubricant *A*, and within the examined driving

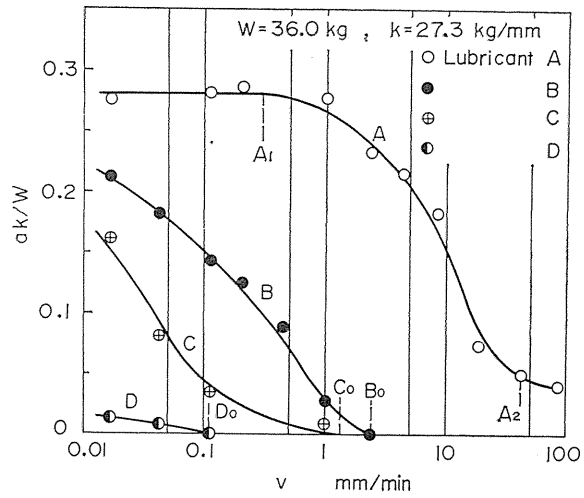

Fig. 8. Amplitude-driving speed curves for various lubricants.

speed, a range in which a becomes nearly constant does not appear. It is seen that the amplitude a decreases abruptly as the driving speed v increases, and htɛt in the range beyond the speeds B_0, C_0, D_0, as shown in the figure for the individual lubricant, the stick-slip motion disappears and the slider moves smoothly.

Figure 9 illustrates variation of the stick-slip frepuency with increase of the driving speed, which coresponds to Fig. 8. In the figure, the frepuency f is represented in the non-dimensional form f/f_0, where f_0 is the natural frepuency of the

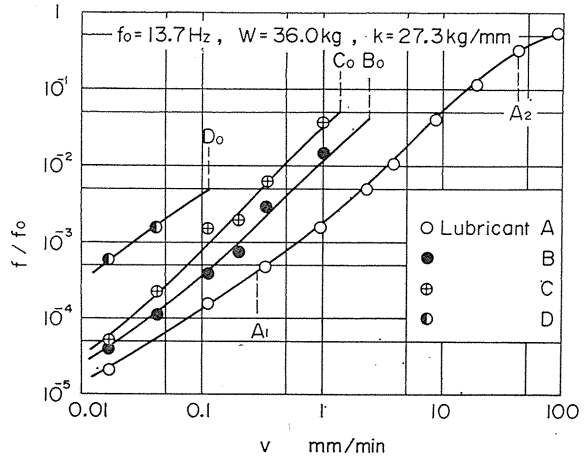

Fig. 9. Frequency-driving speed curves for various lubricants.

system which is calculated from the stiffness k of the driving system and the weight W of the slider, that is, $f_0=\sqrt{gk/W}/(2\pi)$. It is seen in Fig. 9 that the frequency of the stick-slip motion increases as the driving speed v increases in general and the tendency that f/f_0 is convergent to unity (f is convergent to f_0)

as the driving speed increases is recognized in the case of the lubricant A. Meanwhile, in the case of lubricants B, C and D, the stick-slip motion disappears at speeds B_0, C_0 and D_0 as shown in Fig. 8 at which the frequency f is considerably smaller than f_0. Moreover, comparing Fig. 9 with Fig. 8 in the case of lubricant A, the feature of the increasing rate of frequency varies with the range of driving speed, that is, the range below A_1, between A_1 and A_2, beyond A_2. Under the conditions of lower driving speed, the relation $f_0=v/2a$ ($f=1/T_1$, $T_1=2a/v$) holds approximately because the stick time T_1 is considerably larger than the slip time T_2. Therefore, at the speed below A_1, it is recognized that f is approximately proportional to v because the amplitude a is nearly constant as shown in Fig. 8. At the speed between A_1 and A_2 the increasing rate of f is larger than that at the speed below A_1, because a decreases abruptly as v increases. At the speed beyond A_2, owing to the fact that T_1 approaches T_2 in magnitude, the slider makes a nearly harmonic self-excited oscillation, the frequency of which approaches the natural frequency f_0 of the system, and as a result, f/f_0 is considered to be convergent to unity at the range of the higher driving speed.

Figures 10 and 11 show the characteristics of the stick-slip motion at different weights of the slider. It is seen in Fig. 10 that the magnitude of the amplitude a increases as the weight W increases. The value of ak/W increases as the weight W increases and this fact implies that the amplitude is not proportional to the weight W and the influence of the weight on the amplitude is complicated. Moreover, it is seen that the critical driving speed at which the stick-slip motion disappears becomes higher as the weight increases in general and this tendency is

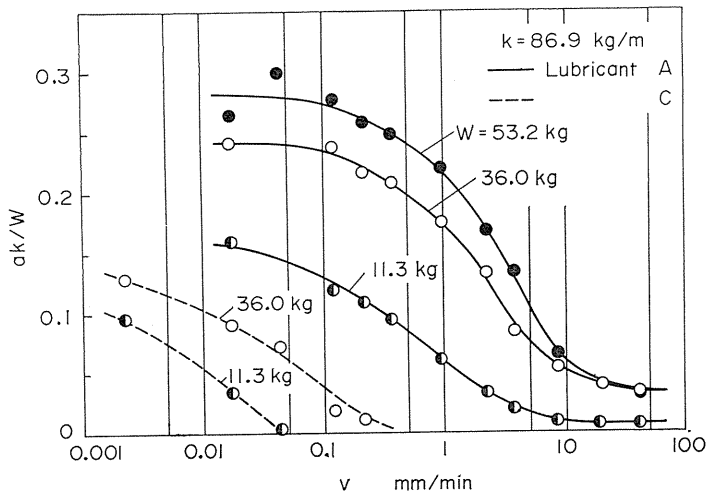

Fig. 10. Amplitude-driving speed curves for various weight of slider.

remarkable in the case of the lubricant C. It is seen in Fig. 11 corresponding to Fig. 10 that the frepuency f decreases as the weight increases, and that the speed at which frequency f is convergent to f_0 becomes higher as the weight increases.

Figures 12 and 13 show the characteristics of the stick-slip motion at different stiffness of the driving system. It is seen in both the figures that as the stiffness

increases the amplitude decreases and the frepuency increases, and that the increases of the stiffness is equivalent to the decrease of the weight with respect to the characteristics of the stick-slip motion.

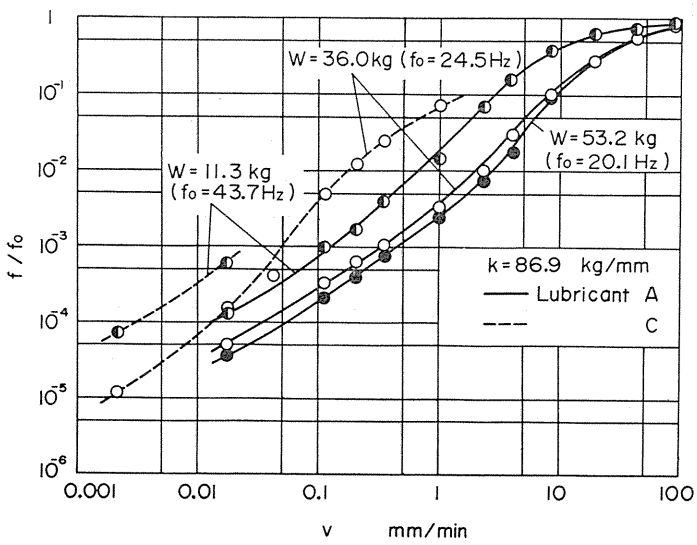

Fig. 11. Frequency-driving speed curves for various weights of slider.

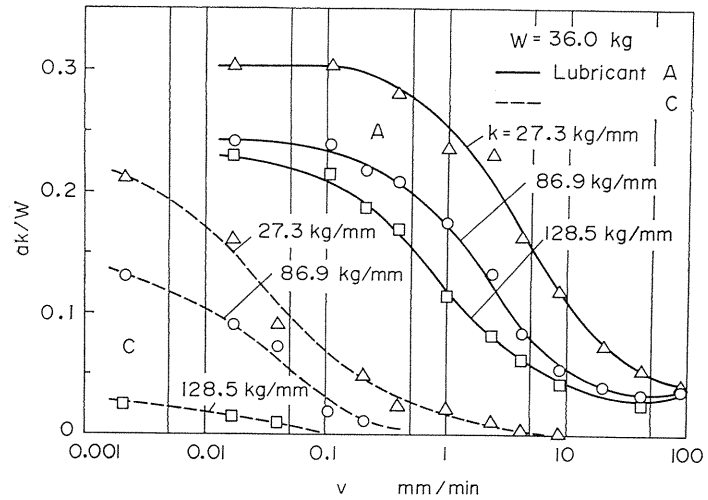

Fig. 12. Amplitude-driving speed curves for various stiffnesses of spring.

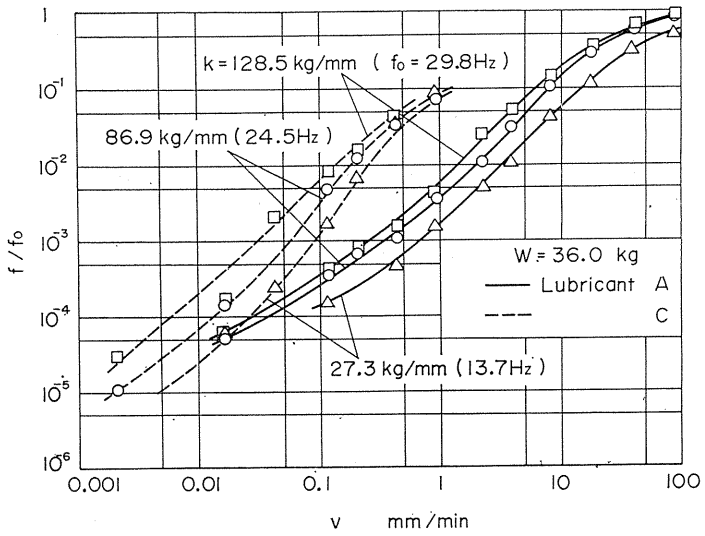

Fig. 13. Frequency-driving speed curves for various stiffnesses of spring.

2. 3. Conlusion

It is clear that the vibratory characteristics of the slider vary with the properties of the applied lubricant and the driving system. It is considered that the variation in the dynamic characteristics is due to the fact that the frictional properties of the slideway at the static and the kinetic conditions are affected markedly by the kind of lubricant applied and the vibratory properties of the system. The frictional properties of the slideway will be discussed in the later parts in detail.

3. Static Friction in Stick-Slip Motion

3. 1. Properties of Static Friction

The slip motion of the slider which has rested on the slideway occurs at the moment when the driving force acting on the slider overcomes the maximum frictional force. Referring to Fig. 6, it may be considered that the maximum frictional force F_0 is equal to the maximum spring force kx_2 at the point B in the figure where the slider begins the slip motion.

Figures 14 and 15 show the relation between the stick time T_1 and maximum frictional coefficient ($\mu_0=F_0/W$) which is calculated from kx_2, that is, the maximum frictional force F_0. In the figures, $T_1\sim\mu_0$ relations in the case of lubricants A and C are shown collectively at different weights of the slider and at different stiffnesses of the driving spring. From the figures, it is evident that μ_0 increases as T_1 increases, and that the increasing rate of μ_0 diminishes as T_1 increases, μ_0 then converges to a certain value for the longer stick time. Furthermore, it is seen that the relative amount of μ_0, the required time for μ_0 to converge to a certain value and the convergent value of μ_0 are affected strongly by the kind of lubricant applied. Namely, for the lubricant A, the range of variation of μ_0 with

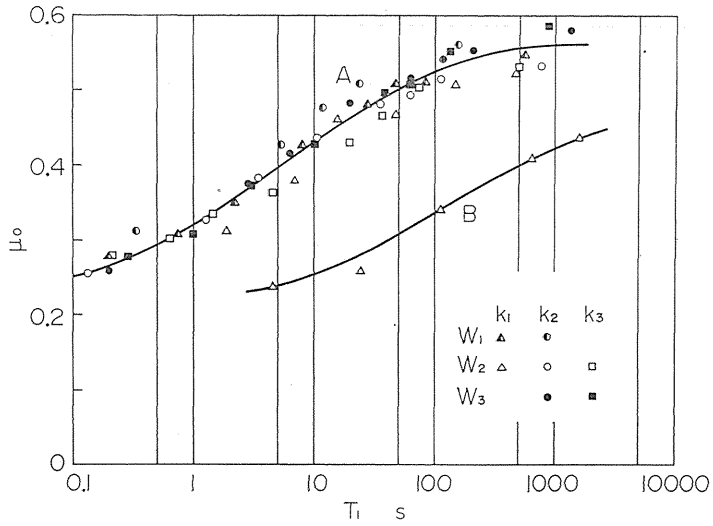

Fig. 14. Time effect on static frictional coefficient.

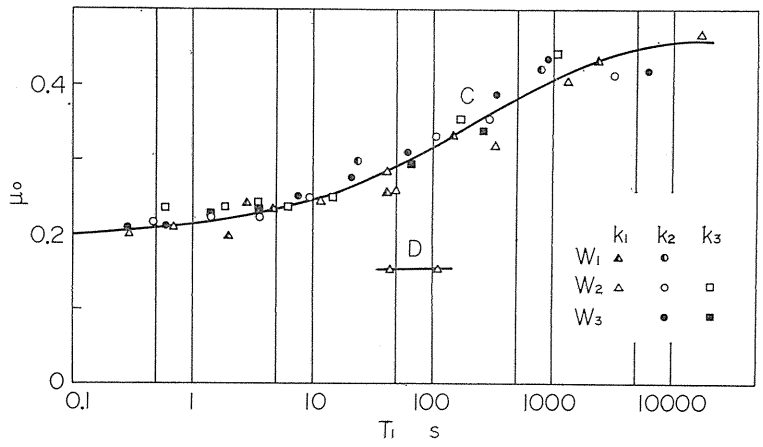

Fig. 15. Time effect on static frictional coefficient.

T_1 is larger than that for other lubricants, and μ_0 is converging at the smaller value of T_1, and the convergent value of μ_0 is large. Moreover, it is seen that for both the lubricants A and C, μ_0 is barely affected by the weight of the slider and the stiffness of the driving system within this experiment. From these results, it may be considered that μ_0 can be represented numelically as a function of T_1 only.

The frictional condition of the slideway in this experiment must be the so-called boundary lubrication, considering that the sliding speed is low, the finished surfaces are relatively rough, and the frictional coefficients observed are fairly large. The time-dependence of static friction thus appears closely associated with the transitional condition of boundary lubrication on the slide surfaces.

3. 2. *Formulation of Static Friction*

Here, an empirical formula is proposed for quantitative treatment of the time-dependence of static friction. Up to now, several attempts have been made to formulate the time-dependence of μ_0 as shown in Table 3. Howe, et al.[7], have

Table 3. Formulas from various researchers

Researchers	Formulas	μ_s	μ_d	Other parameters
Howe	$\mu_0=\mu_d+(\mu_s-\mu_d)(1-e^{-CT})$	0.56	0.21	$C=0.99$
			0.20	$C=0.0058$
Derjaguin	$\mu_0=\mu_d+C_1T/(C_2+T)$		0.21	$C_1=0.32,\ C_2=2.00$
			0.20	$C_1=0.26,\ C_2=200$
Rabinowicz, Rlockley	$\mu_0=\mu_d+C_1T^{C_2}$		0.21	$C_1=0.11,\ C_2=0.23$
			0.20	$C_1=0.021,\ C_2=0.33$
Okamura	$\mu_0=\mu_s/\{(\mu_s/\mu_d-1)/\sqrt{CT+1}+1\}$	0.56	0.21	$C=5.0$
		0.45	0.20	$C=1.0$

upper colum ; Lubricant *A*
lower colum : Lubricant *C*

measured Van der Waal's attractive forces between glass surfaces and found the strong time-dependence of this force. From such results, a formula has been suggested. Derjaguin[8] has examined the critical conditions for occurrence of the stick-slip motion, and proposed a formula for $\mu_0 \sim T_1$ relation on the basis of the experimental facts, that static frictional coefficient increases with the stick time, and that μ_0 tend to a certain value for an extended stick time. Rabinowicz[9] has also proposed an empirical formula on the basis of experimental results. Brockley, et al.[5], have given a good explanation for the time-dependence of static friction by using the creep theory on the metallic junctions, and expressed the $\mu_0 \sim T_1$ relation in the same formula as Rabinowicz. However, these formulas are derived from dry frictional condition and are not in through agreement with experiments over a wide range of stick time. For lubricated conditions, Okamura[10] has explained the time-dependence of static friction by the "squeeze" theory. He derived a formula for the $\mu_0 \sim T_1$ relation theoretically under lubricated conditions by assuming that the static frictional coefficient is inversely proportionate to the lubricant film thickness which varies with stick time through the squeeze film effect. This simple assumption, however, may be invalid because in that only the variation of the lubricant film thickness is considered, while the relation between the film thickness and contact is not taken into account.

Figure 16 shows $\mu_0 \sim T_1$ relation by these formulas. The values of the parameters in the equations are summerized in Table 3. The figure shows that the formulas by Rabinowicz and Brockley are limited to the narrow applicable range of the stick time. Howe's formulas provides a good explanation of the time-dependence of static friction but the applicable range is still restricted, while Okamura's formulas gives good agreement with the experimental results.

In this study an empirical formula is proposed, similar to Howe's equation, which has a wider application of T_1. The expression is

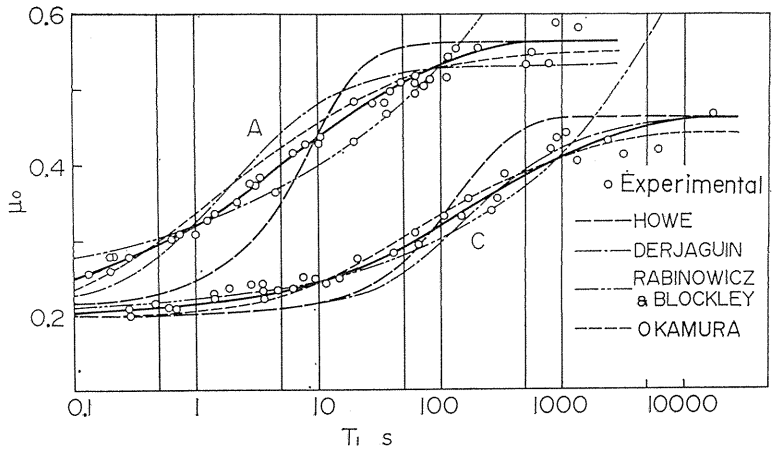

Fig. 16. μ_0-T_1 curves from various researchers.

$$\mu_0=\mu_s-(\mu_s-\mu_d)e^{-\gamma T_1{}^m} \tag{1}$$

where,

μ_s=asymptotic value of μ_0 when $T_1\to\infty$,

μ_d=value of μ_0 when $T_1\to 0$ and nearly equal to kinetic friction,

γ, m=constants which depend on properties of lubricant applied and the surface topography, as described later.

Figure 17 shows the results calculated by equation (1) so as to apply the equation to the experimental results. In these cases, the values of μ_s, μ_d, γ, and m

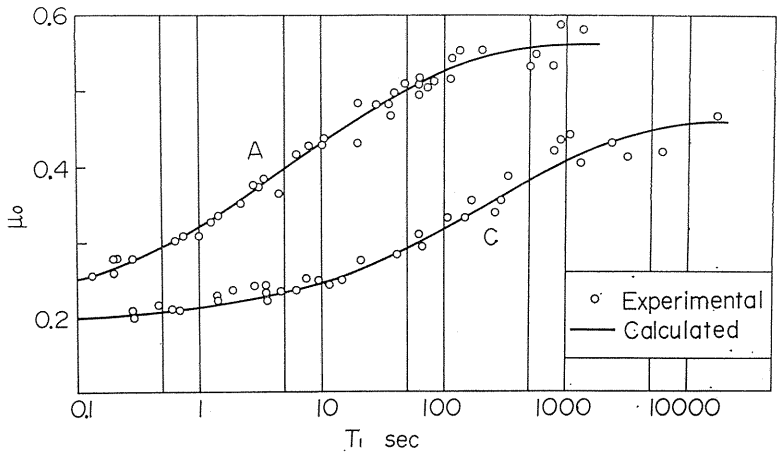

Fig. 17. Calculated μ_0-T_1curves.

for the various applied lnbricants are summerized in Table 4, where μ_s and μ_d are both obtained by experiments. The calculated $\mu_0\sim T_1$ curves show good agreement with experimental results as seen in Fig. 17; and the time-dependence of static

friction can be well expressed by equation (1) for a wide range of stick time.

Table 4. Chart of parameter

Lubricants	μ_s	μ_d	γ	m
A	0.56	0.21	0.38	0.40
C	0.46	0.20	0.067	0.45

3. 3. Conclusion

Based on the experimental results, in order to make the stick-slip process clear, the characteristics of the static friction in the stick period concretely. As a result, it has been shown that the static frictional coefficient generally increases with the increases of the stick time, and that the magnitude of the frictional coefficient and its increasing property vary remarkably with the kind of lubricant applied, and further that the static frictional coefficient is independent of the weight of the moving element and the stiffness of the driving system. On the bases of these experimental results, an expression for the static frictional coefficient μ_0 is proposed, in which μ_0 can be expressed with a simple exponential formula by the stick time.

4. Kinetic Friction in Stick-Slip Motion

4. 1. Relation between Stick-Slip Motion and Kinetic Frictional Force

Referring to Fig. 5, the equation for slider motion in slip period is

$$M\ddot{y}=kx-F \tag{2}$$

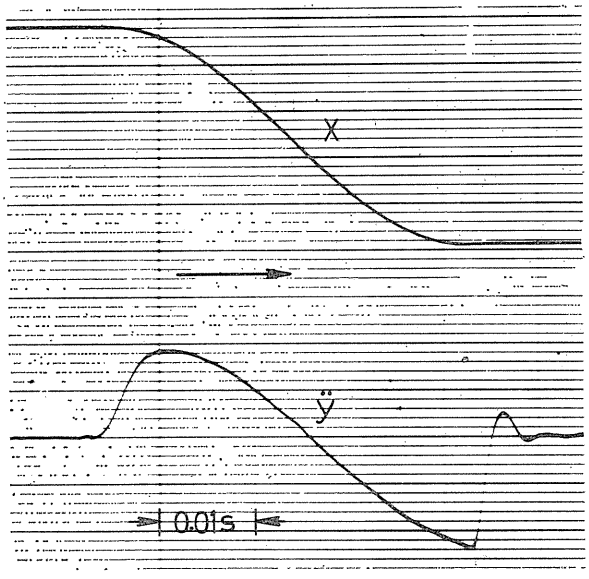

Fig. 18. Experimental records of slip motion.

Cosequently, the momentary frictional force of the slideway may be investigated by measuring the deflection x of the driving spring and the sliding acceleration $\ddot{y}$ of the slider. An example of the experimental records of x and $\ddot{y}$ as measured by a strain gauge attached to the driving spring and accelerometer on the slider is shown in Fig. 18.

Figure 19 shows an example of the relation between the momentary "slip" speed $\dot{y}$ and the kinetic frictional coefficient μ which is obtained from the experimental records such as Fig. 18. In the figure, it is seen in general that the frictional coefficient shown in 1 at the beginning of the slip motion, which indicates maximum frictional coefficient μ_0, has an extremely large value, and that the value of μ decreases rapidly as indicated by 1-2-3 with the rise of $\dot{y}$ and after the value of $\dot{y}$ reaches point 3, which indicates a maximum slip speed, μ is nearly constant in spite of $\dot{y}$ decreasing as shown in 3-4-5. In the case of higher driving speed, μ_0 is small and the value of μ in the period of acceleration is small, but in the period of deceleration μ is held in nearly constant value which seems to be independent with the value of μ_0.

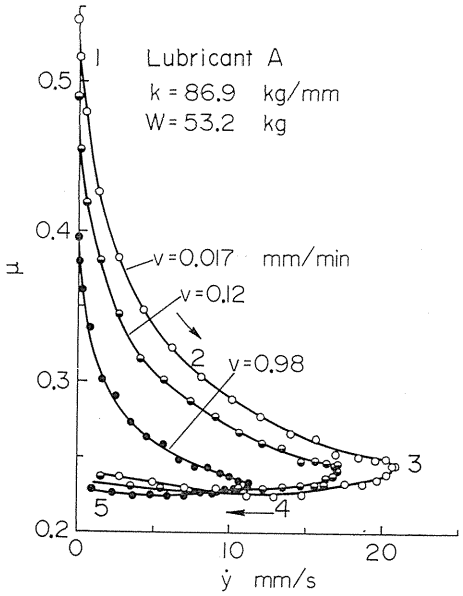

Fig. 19. Relation between slip speed and frictional coefficient.

Figure 20 shows $\mu \sim \dot{y}$ relations in the case of different lubricant applied. In the figure, the general tendency of change in μ is same as in Fig. 19, but it is found that the value of μ and the decreasing rate of μ with the rise of $\dot{y}$ is remarkably different by the lubricant.

Figures 21 and 22 show the relation between the displacement y of the slider in the slip motion and μ obtained from Figs. 19 and 20 respectively. In the figures, it is seen that μ is considerably affected by the driving speed and the kind of the lubricant applied in the same manner as shown

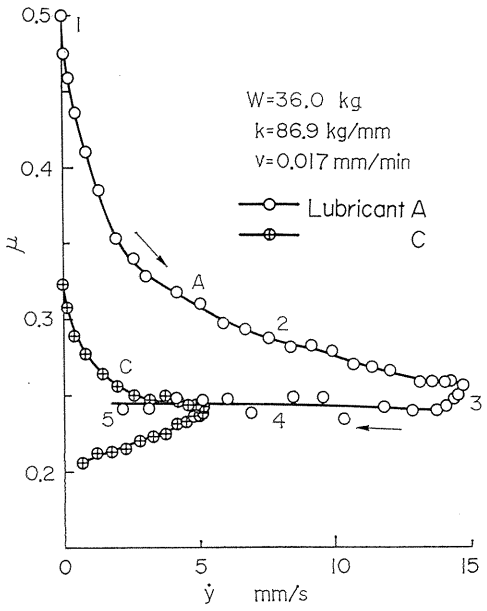

Fig. 20. Relation between slip speed and frictional coefficient.

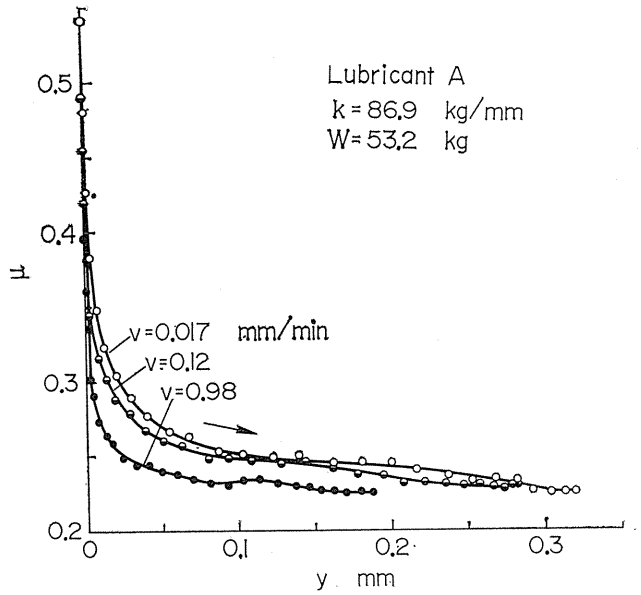

Fig. 21. Relation between slip distance and frictional coefficient.

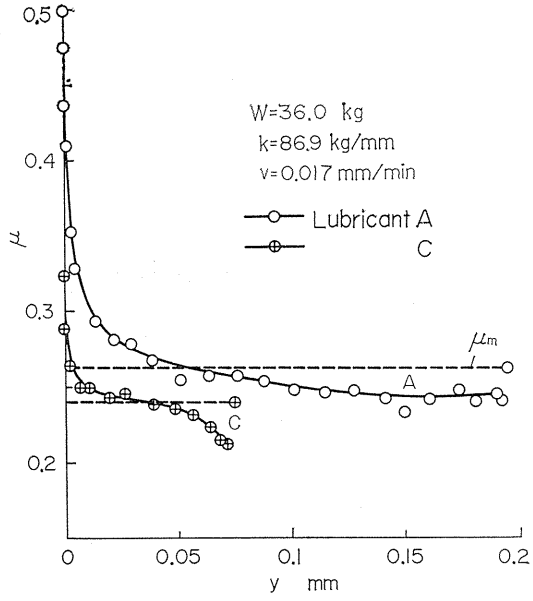

Fig. 22. Relation between slip distance and frictional coefficient.

in Figs. 19, 20. It is recognized that the kinetic frictional force in the slip period shows a complicated transitional property becaues the slip speed changes over a wide range in a short time, and it is considered that the value of μ and that changing tendency are affected not only by the driving speed and the lubricant applied but also by the sliding conditions such as the vibratory property of the driving system.

Here, in order to understand summarily the relations between the sliding conditions and the kinetic frictional coefficient which shows the complicated transitional property as shown in Figs. 19, 22, mean kinetic frictional coefficient in the slip period is calculated as a representative value of the kinetic frictional coefficient.

Figure 23 shows the relation between the changing process of the frictional force accompanied with the slip motion and the mean frictional force. In the figure,

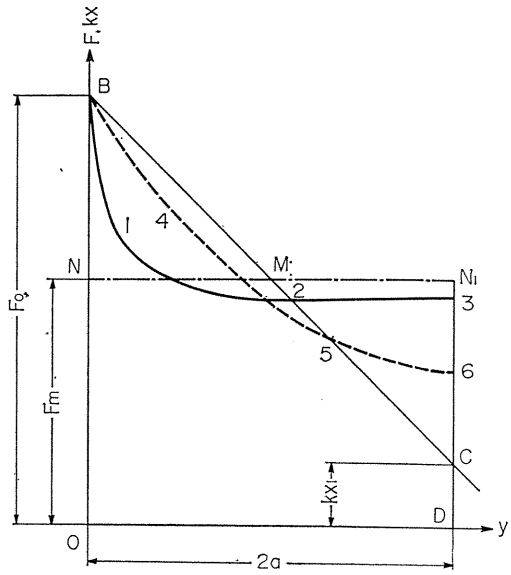

Fig. 23. Schematic diagram of mean frictional force.

when the driving speed is low and the slip time is much shorter than the stick time, the driving spring force decreases along the straight line *BMC* while the slider slips from 0 to *D*. In this case, the slip motion corresponds to *BC* in Fig. 6 and the slip distance is equal to twice the amplitude of the stick sllp motion. If the frictional force in the slip period changes along the curve *B*-1-2-3 (or *B*-4-5-6) in the figure, the elastic potential energy of the driving spring which corresponds to 0-*B*-*C*-*D* is converted to frictional work in the slip period, and both are nearly equal. Consequently, the mean frictional force *Fm* may be represented by the line NMN_1 which passes through the middle point *M* of *BC*. In this meaning, the mean frictional force in the slip period can be calculated as the mean value of the maximum and the minimum spring force approximately.

Figure 24 shows the relation between the characteristics of the static and kinetic friction and the stick-slip motion. In the figure, the curve *AB* shows the relation between the stick time T_1 and maximum static frictional coefficient μ_0, as shown before. If the slider is driven at a constant speed, the driving force acting upon the slider which is under the stick condition increases along the straight line 01, and the inclination of this line is indicated by *kv/W*. At the point 1 whehe the line 01 crosses the curve *AB*, the spring force is equal to ohe maximum frictional force. When the spring force exceeds the point 1, the slider begins to slip. It is

considered from the physical law between the potential energy of the spring and the frictional work that the slider moves from point 1 to point 2, the distance between both points being equal to twice the distance between 1 and M_1, where M_1 is the mean frictional coefficient in the slip period; and then the slider attaines the stick condition. The spring force increases again along the straight line 34 which is parallel to line 01, and next the spling force changes with the process 4-5-6. Finally, the stick-slip motion of the slider occurs in the steady cycle as shown in *P-Q-R*.

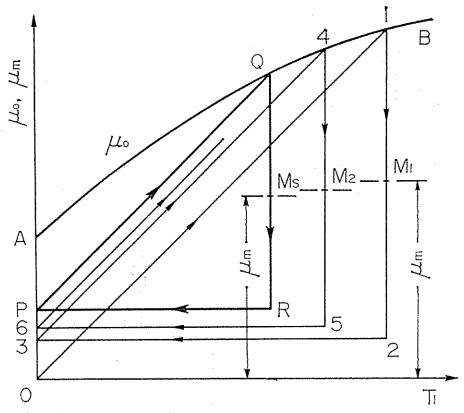

Fig. 24. Relation between frictional coefficient and stick slip motion.

4. 2. *Properties of Kinetic Friction and its Formulation*

From the fact mentioned above, it is obvious that the magnitude of the mean kinetic frictional coefficient μ_m is one of the most important factors which govern closely the properties of the stick-slip motion, in addition to μ_0. However, it is considered that the value of μ_m is affected by the various sliding conditions. As factors influencing the kinetic frictional coefficient μ_m, there are the maximum speed of the slip motion, the slip time, the weight of the slider and the maximum frictional coefficient at the beginning of the slip motion in addition to the properties of the lubricant applied. Here, the influence of these factors on μ_m is discussed in detail.

Figures 25 and 26 show relations between maximum slip speed and μ_m as obtained from the experiment with both lubricants *A* and *C* under various conditions, that is,

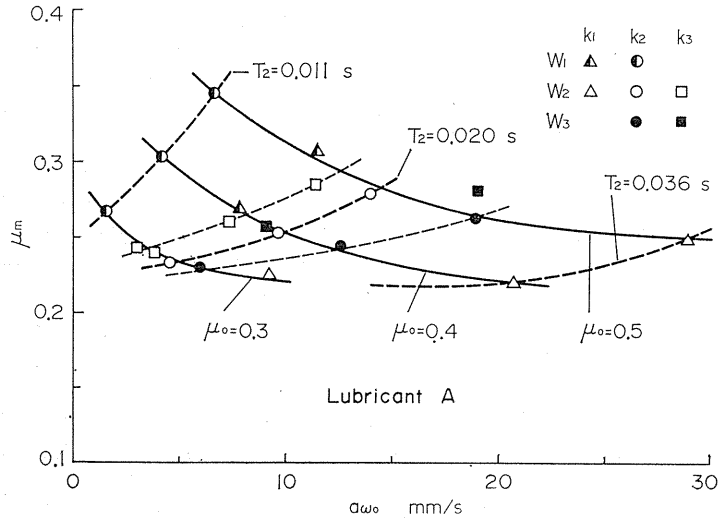

Fig. 25. Relation between $a\omega_0$ and μm.

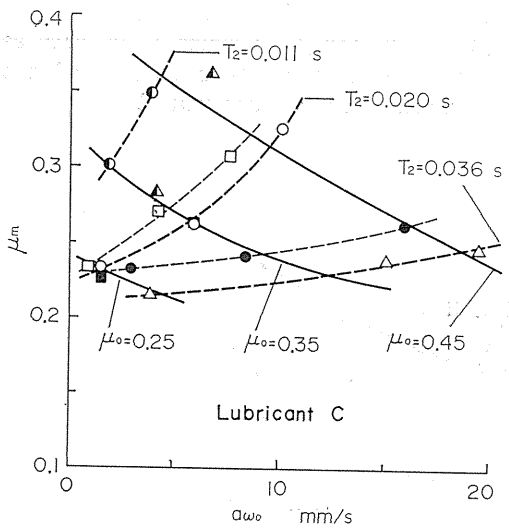

Fig. 26. Relation between $a\omega_0$ and μm.

by changing the weight W of the slider, the stiffness k of the driving spring and the driving speed. Since the slip motion of the slider may be regarded as having behaviour similar to a free oscillation of the system, the maximum slip speed is represented by $a\omega_0$, where a is the amplitude of the stick-slip motion and ω_0 is the natural frequency of the system which is determined by W and $k(\omega_0=\sqrt{gk/W})$. From both figures, in the case where μ_0 is taken as a parameter, μ_m shows a negative tendency for μ_m to decrease as $a\omega_0$ increases. On the other hand, where the slip time T_2 is taken as a parameter, μ_m show the positive tendency for μ_m to increase as $a\omega_0$ increases. These contradictory characteristics of μ_m are due to the fact that the factor $a\omega_0$ can not vary independently of the oter factors, and various factors depend on each other. Consequently, it is considered possible that some of the other factors besides $a\omega_0$ influence μ_m more significantly. In order to reveal the extent of the influence of each factor, the relations between each factor and μ_m are studied in a manner similar to Figs. 25 and 26. The arranged date are given in Table 5. In the table,

Table 5. Analysis of factors which influence μ_m

	Vari-ables	Para-meters	Effect on μ_m						Vari-ables	Para-meters	Effect on μ_m				
			$a\omega_0$	a	μ_0	T_2	W				$a\omega_0$	a	μ_0	T_2	W
1	$a\omega_0$	a	+	C	+	−		11		T_2	+	+	+	C	
2		μ_0	−	−	C	−		12		W	+	+	+	C	
3		T_2	+	+	+	C		13	T_2	$a\omega_0$	C	−	+	−	
4		W	+	+	+	−	C	14		a	+	C	+	−	
5	a	$a\omega_0$	C	−	+	−		15		μ_0	−	−	C	−	
6		μ_0	−	−	C	−		16		W					C
7		T_2	+	+	+	C		17	W	$a\omega_0$	C	−	+	−	−
8		W	+	+	+		C	18		a	+	C	+	−	−
9	μ_0	$a\omega_0$	C	−	+	−		19		μ_0	−	−	C	−	−
10		a	+	C	+	−		20		T_2				C	

C : Parameter itself

such factors showing a steady influence on μ_m independently of the other paramaters can be thought to influence μ_m considerably. From this viewpoint, in Table 5, it is seen that the maximum frictional coefficient μ_0 and the slip time T_2 are the most

significant factors influencing μ_m in the case of either lubricant A or C.

Figures 27 and 28 show the relations between μ_0 and μ_m in which T_2 is taken as a parameter. In both figures, it is seen that μ_m increases as μ_0 increases and the extent of the influence of μ_0 on μ_m is more marked for the lubricant C.

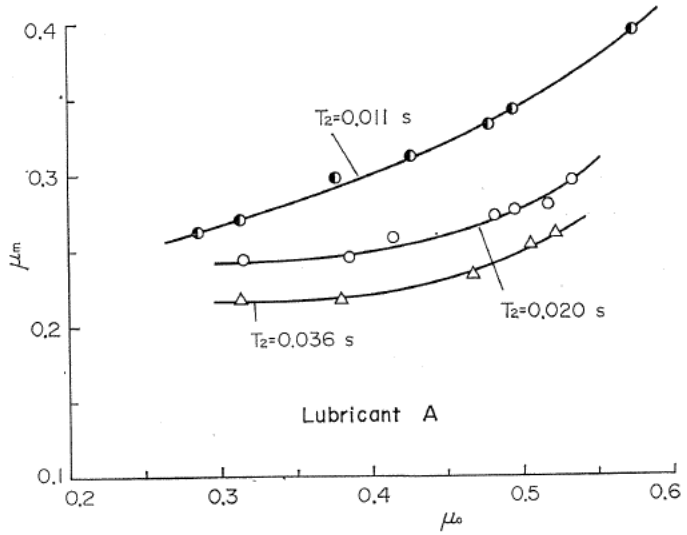

Fig. 27. Relation between μ_0 and μm.

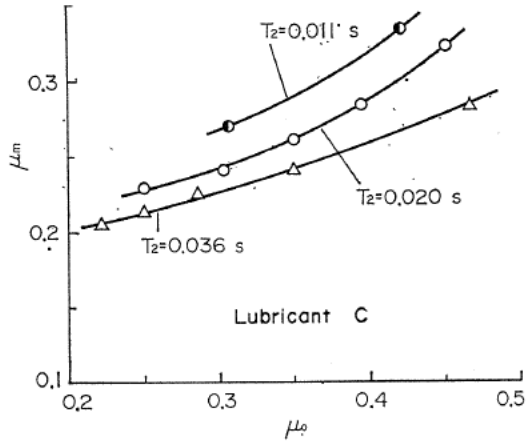

Fig. 28. Relation between μ_0 and μm.

Figures 29 and 30 show the relations between T_2 and μ_m, in which μ_0 is taken as a parameter. In bot figures, it is seen that μ_m decreases with the increase of T_2, and the difference in μ_m originating from the difference in μ_0 grows gradually and μ_m approaches a constant value independent of μ_0 as T_2 increases. For the lubricant A, it is seen that the decreasing rate of μ_m in conjunction with the increase of T_2 is higher than for the lubricant C, and that at a relatively large T_2

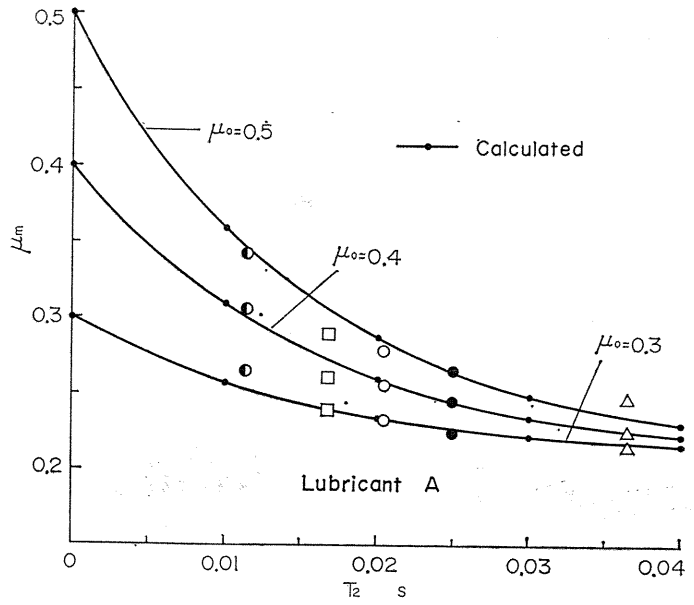

Fig. 29. Relation between T_2 and μm.

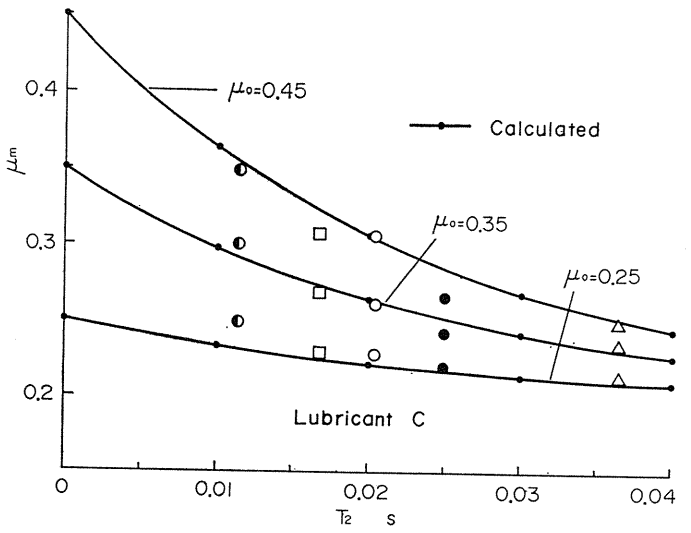

Fig. 30. Relation between T_2 and μm.

the influence of same becomes small and μ_m approaches a constant value.

From the foregoing, it is clear that the characteristics of the kinetic friction in the slip period may be understood all-inclusively by introducing a concept of the mean kinetic frictional coefficient μ_m, and the factors which influence μ_m are μ_0 and T_2 in the first meaning.

Here, in order to understand the characteristics of the kinetic friction during

the slip motion quantitatively, an expression for μ_m is proposed corresponding to the empirical expression for μ_0.

$$\mu_m=\mu_d+(\mu_0-\mu_d)^{-\delta T_2^n} \tag{3}$$

In equation (3), μ_d represents the value which μ_m approaches when $T_2\to\infty$, and it is considered to be the same parameter as the one in equation (1) for static friction. The value of δ and n are the measure of the time effect for μ_m, and they are decided by the correlation between the lubricant and the surface topography of the slideway, the properties of δ and u being considered to be similar to the properties of γ and m respectively.

On the basis of the experimental results with stick-slip motion, the parameters shown above are determined as in Table 6 for the lubricants *A* and *C*. Calculated

Table 6. Parameters in expression for kinetic friction

Lubricants	μ_d	δ	n	μ_s	γ	m
A	0.21	67	1	0.56	0.38	0.40
C	0.20	43	1	0.46	0.067	0.45

values of μ_m using equation (3) are shown concurrently in Figs. 29 and 30. In the figures, the calculated values agree well with the experimental values of μ_m, and it is confirmed that the characteristics of μ_m are well expressed by equation (3).

4. 3. Conclusion

The characteristics of the kinetic friction in the slip period are discussed. The result is clarification of the characteristics of the kinetic friction as understood collectively by introducing the concept of mean kinetic frictional coefficient μ_m.

The factor which influence the value of μ_m are studied in detail, and then it is revealed that the properties of the lubricant, the maximum frictional coefficient at the beginning of the slip motion and the magnitude of the slip time influence μ_m significantly, and a generalized expression for μ_m is proposed.

5. Critical Condition of Occurrence of Stick-Slip Motion

5. 1. Estimation of Stick-Slip Motion

On the basis of the expressions for static and kinetic friction with the slideway and the relation between the frictional characteristics and the stick-slip motion shown in Fig. 24, the characterics of the stick-slip motion are discussed quantitatively.

Substituting equation (1) into equation (3), the following equation is given.

$$\mu_m=\mu_d+(\mu_s-\mu_d)(1-e^{-\gamma T_1^m})e^{-\delta T_2^n} \tag{4}$$

Referring to Fig. 24, the amplitude of the stick-slip motion is as follows:

$$a=(\mu_0-\mu_m)W/k=T_1v/2 \tag{5}$$

Substituting equation (1) into equation (5). the relation between v and T_1 is obtained as follows:

$$kvT_1/2W=(\mu_s-\mu_d)(1-e^{-\gamma T_1^m})(1-e^{-\delta T_2^n}) \tag{6}$$

where

$$T_2=1/2f_0=\pi\sqrt{W/gk} \tag{7}$$

The amplitude a of the stick-slip motion can beobtained from equations (6) and (5). That is, equation (6) is converted to following equations to be resolved graphically.

$$\left.\begin{aligned} y_1&=kvT_1/2W(\mu_s-\mu_d)(1-e^{-\delta T_2^n})\\ y_2&=1-e^{-\gamma T_1^m}\end{aligned}\right\} \tag{8}$$

The stick time T_1 corresponding to a given value of v is obtained as the point of intersection of the straight line y_1 (the inclination of y_1 is proportional to v) and the curve y_2 as shown in Fig. 31, and then the amplitude a is obtained from equation (5).

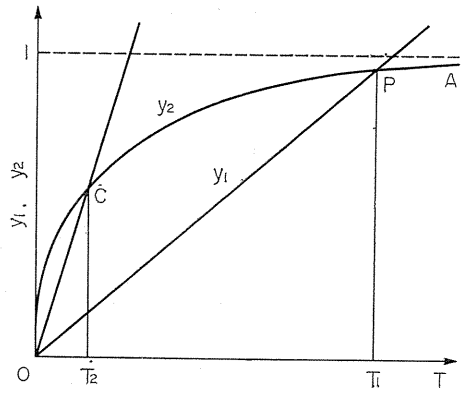

Fig. 31. Graphical calculation of T_1.

Figures 32 and 33 show the calculated results of the amplitude in non-dimensional form for both the lubricants A and C where W and k are varied as obtained by the above mentioned method.

For the lubricant A, the experimental results are shown in the figure together with the calculated results. It is recognized in the figures that the calculated results agree very well with the experimental results. Therefore, by the application of the expressions (1) and (3) for the static and kinetic friction the characteristics of the stick-slip motion are well obtained quantitatiuery. Moreover, the motion of the slider in the slip period can be estimated by employing the mean kinetic frictional coefficient.

In equation (2) which expresses the equation for slider motion in the slip period, the slip distance y is given referring to Fig. 6 as follows:

$$y=x_2-x+vt \tag{9}$$

Consequently, equation (2) can be transformed as follows:

$$M\ddot{x}+kx=\mu_m W \tag{10}$$

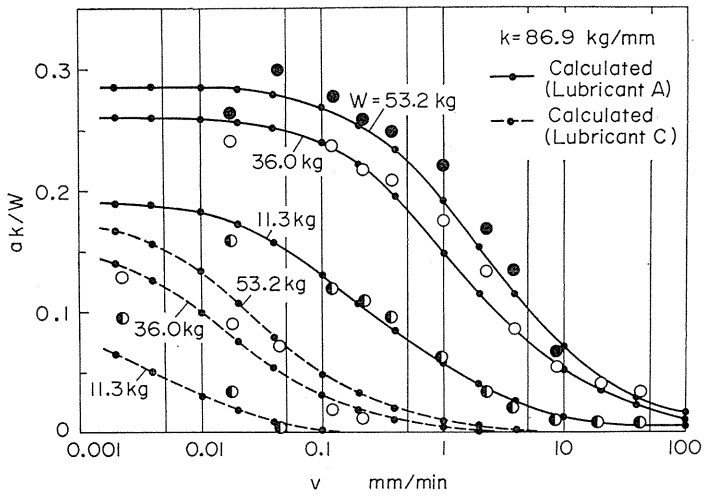

Fig. 32. Calculated amplitude-driving speed curves for various weights of slider.

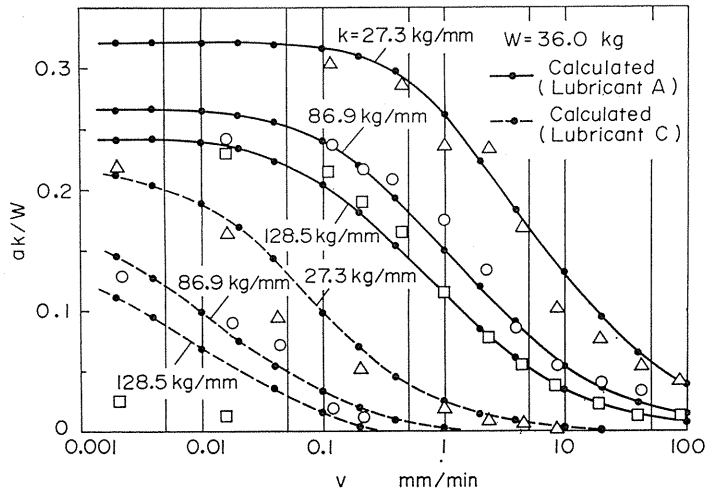

Fig. 33. Calculated amplitude-driving speed curves for various stiffnesses of driving spring.

Under the initial condition

$$\begin{cases} x = x_2 = \mu_0 W/k \\ \dot{x} = 0 \end{cases}$$

$$\text{at } t = 0$$

Equation (10) can be solved as

$$x = \{(\mu_0 - \mu_m)\cos\omega_0 t + \mu_m\} W/k \tag{11}$$

where

$$\omega_0 = \sqrt{gk/W}$$

It is recognized from equation (11) that with the deflection x of the spring the slider motion in the slip period is an harmonic oscillation having the amplitude $(\mu_0 - \mu_m)W/k$.

Such a calculated result of the slip motion is compared with the experimental one. Figures 34 and 35 show examples of the phase plane trajectories, the abscissa indicates the ratio of the deflective speed $\dot{x}$ of the driving spring spring (which is nearly equal to the slip speed of the slider, since the driving speed is far lower the slip speed) in relation to the angular natural frequency ω_0 of the driving system, and the ordinate indicates the deflection x of the spring. The experimental results are obtained from experimental records as in Fig. 18, and the calculated results are obtained as with the foregoing methods on the basis of the experimental values of μ_0 and μ_m.

In Fig. 34, as the driving speed v is smallar than the slip speed $\dot{y}$, the stick process is shown as the straight line RQ which coincide with the abscissa, and the slip motion is shown as the curve QR.

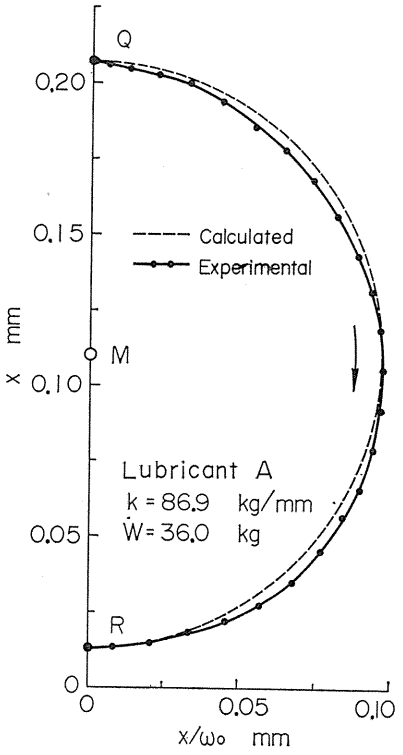

Fig. 34. Phase plane trajectory of stick-slip motion.

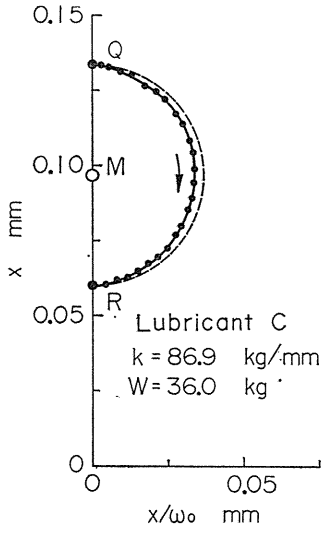

Fig. 35. Phase plane trajectory of stick-slip motion.

From both figures, it is recognized that the calculated results coincide very well with the experimental results and that the slip motion of the slider can be estimated with sufficient accuracy by employing of the concept of the mean kinetic frictional coefficient.

5. 2. Critical Condition of Occurrence of Stick-Slip Motiou

The critical condition for occurrence of the stick-slip motion is discussed. The stick time decreases gradually as the driving speed v increases, but referring to Fig. 6, the period T_0 of the stick-slip motion does not become so small as the period T_n of the natural oscillation of the system, hence $T_1 \geqq T_2$ holds. Therefore, critical driving speed v_c for occurrence of the stick slip motion is considered to coincide with where $T_1=T_2$. The value v_c is obtained from inclination of the straight line OC in Fig. 31 as follows:

$$v_c=2(\mu_s-\mu_d)(1-e^{-\gamma T_2^m})(1-e^{-\delta T_2^n}) \tag{12}$$

Figure 36 shows the relation between the natural frequency f_0 and the critical

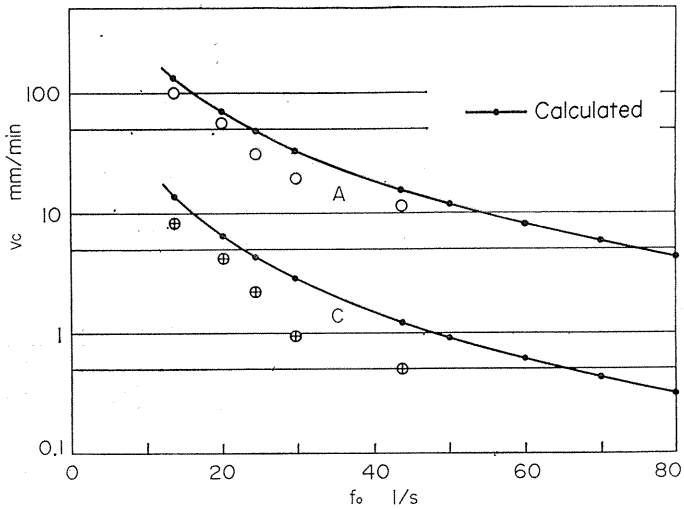

Fig. 36. Relation between natural frequency and critical driving speed of stick-slip motion.

driving speed v_c for the lubricants A and C. In the figure, the value of v_c which is obtained from equation (12) is compared with the value of the experimental critical driving speed beyond which the stick-slip motion disappears in the experiment. It is recognized in general that v_c decreases as f_0 increases. Namely, where the system has a large natural frequency the stick-slip motion is inhibited. Morever, though the value of v_c differs considerably with the kind of applied lubricant, the calculated values of v_c for both lubricants agree well with the experimental value qualitatively. Therefore, it is confirmed that the critical condition for the occurrence of the stick-slip motion can be discussed qualitatively at least using equation (1) and (3).

Next, the relation between the parameters of the friction of the slideway, that is, μ_s, μ_d, γ, m, δ, n, and the critical driving speed is discussed concretely.

Figures 37-41 show examples of the relation between each parameter in the expressions for the frictional characteristics and the critical driving speed v_c which is obtained from equation (12). In Figs. 37, 38, and 39, which show the relation

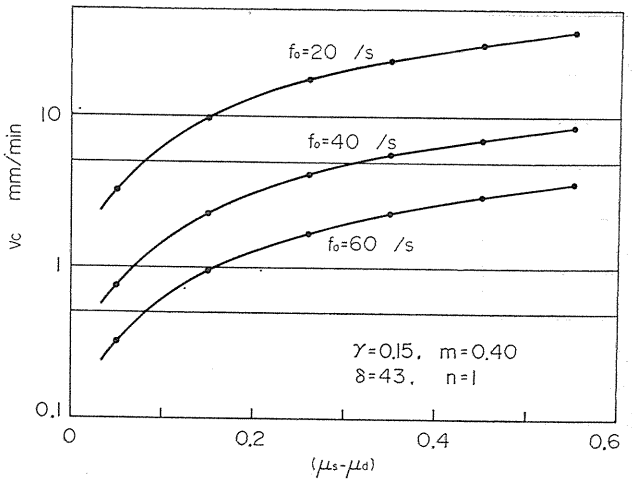

Fig. 37. Relation between $(\mu_s-\mu_d)$ and v_c.

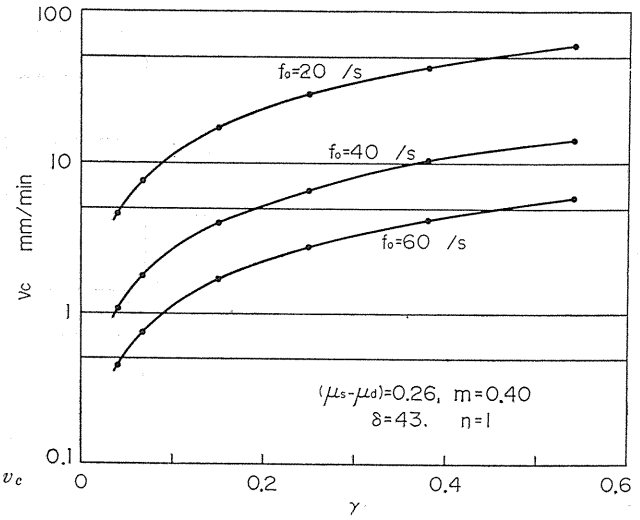

Fig. 38. Relation between γ and v_c

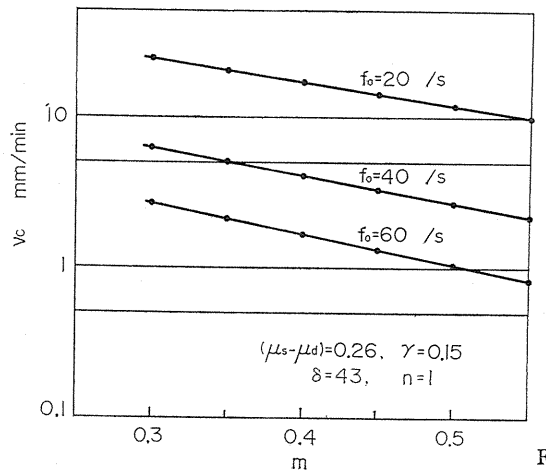

Fig. 39. Relation between m and v_c

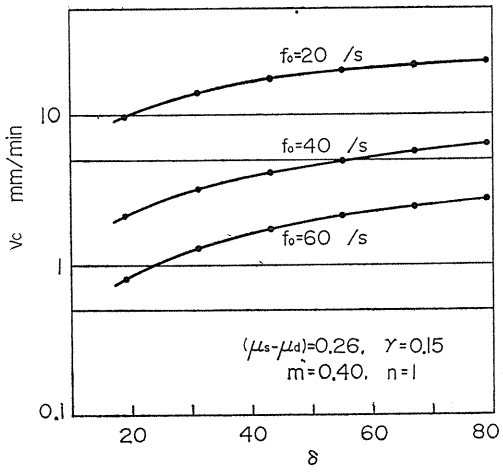

Fig. 40. Relation between δ and v_c.

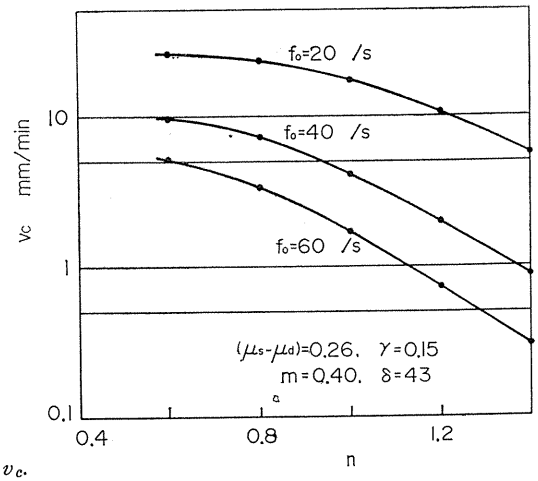

Fig. 41. Relation between n and v_c.

between the parameters for the static friction and v_c, it is seen that v_c increases as the value of $(\mu_s-\mu_d)$ which indicates the variability of μ_0 increases, and that the increasing rate of v_c in terms of the increase of $(\mu_s-\mu_d)$ is large in the range of small value of $(\mu_s-\mu_d)$. It is further seen in general with increasing γ and with decreasing m that v_c increases and the stick-slip motion easily occurs. In Figs. 40 and 41, which show the effect of the parameters for the kinetic friction on v_c, it is seen in general that v_c increases as δ increases and n decreases.

In practice, it can be supposed from these results that a lubricant such as caster oil which is considered to have the high strength as a lubricant film and a high viscosity may show low values of $(\mu_s-\mu_d)$, γ and δ. Consequently v_c is low and the stick-slip motion is prevented, and that probably because the smooth slide-way shows a low value of $(\mu_s-\mu_d)$, γ, δ and a high value of m, n, then v_c is low, too.

From the above, the aptness of the expressions (1) and (3) for the static and

kinetic friction in the stick-slip motion is confirmed, and at the same time it is shown that if these expressions are given, the amplitude and the critical driving speed of the stick-slip motion can be obtained.

5. 3 Conclusion

On the basis of both expessions for static and kinetic friction proposed in Chapters 4 and 5, the characteristics of stick-slip motion namely the amplitude and the frequency can be estimated numerically. A critical condition for occurrence of the stick-slip motion is introduced, hence, the critical driving speed can be calculated and it becomes clear that the calculated results agree well with the experimental results.

6. Pitching and Yawing Motion of Moving Element Caused by Stick-Slip Motion

Irregular behaviour of moving element is also found in the normal direction to the sliding with the stick-slip motion. This irregular behaviour (pitching and yawing motion) creates slight inclination of moving element, and lead to deterioration of machining accuracy.

On the irregular motion in the normal direction to the sliding, Hensen[11], Mitsui[12], Okamura[13], Shiozaki[14], et al. reported some investigations, in which the floating phenomena of the moving element under hydrodynamically lubricated condition were treated both experimentally and theoretically. A machine tool slideway is generally operated under boundary lubricated condition. However, any studies on the pitching and yawing motion under such condition have not been made in spite of its practical importance.

In this Chapter, the fundamental characteristics of the pitching and yawing motion of the moving element accompanied by the stick-slip motion are investigated, and some factors which have influence on the characteristics of the pitching and yawing motion are discussed. The mechanism of that motion is considered too.

6. 1. Experimeutal

The slideway used in this experiment is composed of inverted V and flat shape surfaces as shown in Fig. 42, which was explained in section 2. 1. The pitching and yawing motion of the slider accompanied by the stick-slip motion is measured by five sets of electric micrometers L, which detect the slight displacement of each measuring point $\varepsilon_1 \sim \varepsilon_5$ arranged on the slider. Five pieces of the gauge blocks F which are attached on the slider in the precisely parallel direction to the driving motion are prepared as the base surfaces for the measurement. The measuring points $\varepsilon_1 \sim \varepsilon_3$ are used for detection of the vertical displacement of the slider, and ε_4, ε_5 are used for detection of the horizontal displacement. The position of the projection B, through which the driving force acts on the slider, is changed both vertically and horizontally as F, C_1, C_2, C_3 and V shown in the figure. The position of the standerd driving point C_2 is determined so that the driving force may act on the slider through the center of gravity of it. The point C_1 and C_3 are placed so that the vertical position of them may change. The point V and F are placed so

that horizontal position may change. The experimental conditions are same as shown in Table 1. The lubricants applied are shown in Table 7.

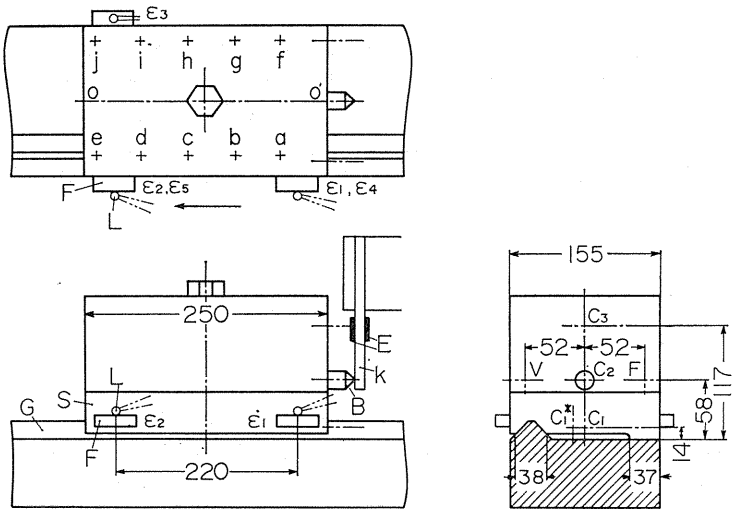

Fig. 42. Experimental apparatus.

Table 7. Lubricants

Lubricants	Viscosity cSt (20℃)	Remarks
A_1	54	Naphthene base mineral oil
A_2	195	〃
A_3	460	〃
B	214	Commercial slideway lubricant
C	1010	Non-drying vegetable oil

The condition of the contact between a machine tool slideway and slider seems to be not always homogeneous over whole contact area. For example, it is laid down in the standard for accuracy of a machine tool such as JIS that a slideway must not be depressed at the middle part, in consideration of deformation by a load and of wear with sliding. In a practical case, a slideway is commonly finished to swelling slightly at the middle part. Thus, it is conceivable that the condition of the contact between the surfaces is more intimate at the middle part than at each end of the slideway.

In order to study the condition of the contact of the slidesurfaces used in this expriment, flatness of both slideway and slider are measured by autocolimater and minimeter at the inverted V and flat shape, respectively. The results of the measurement are shown in Fig. 43 (a) and (b). The curves G and S in the figure show flatness of the surfaces of slideway and slider, respectively. It is found from the

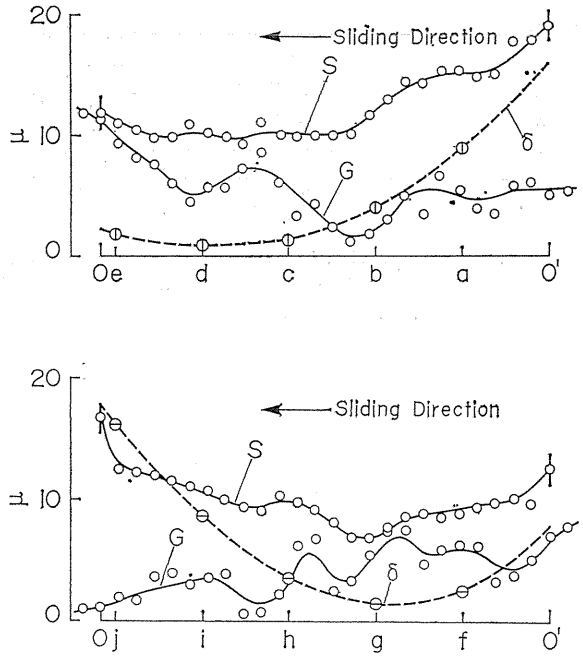

Fig. 43. Flatness of sliding surfaces.

figure that the slider S has a slight swell at the middle in both parts of inverted V and flat, and that the slideway G has good flatness. When these slideway and slider come into contact, the condition of contact between both surfaces seems not to be homogeneous over whole contacting surfaces, and to be more intimate near the top of the swell in both parts V and F. There may be a slight clearance between the surfaces at each end of the slider. Such condition of the slideway used in this experiment is considered to be quite common in reference to the actual machine tool slideway which is provided in accordance with JIS. The broken line δ in Fig. 43 show the amount of the vertical displacement which occurs on the slider when a concentrated load is applied upon the slider at the points a~j (see Fig. 42), and they are considered to indicate the clearance existing between contacting surfaces at each point. The curves δ show good agreement with the nature of the clearance which may be suggested from the difference between flatness curves S and G. Moreover, it is found from the curves δ that both surfaces may contact intimately near the point d at the part V and near the point g at the part F.

6. 2. Properties of Pitching Motion

Figure 44 shows an example of the experimental record of the stick-slip motion and the pitching and yawing motion of the slider. The curve (a) in the figure indicates the stick-slip motion and the group of the curves (b) indicates the pitching and yawing motion of the slider at each measuring point. It is seen from the figure that each measuring point of the slider moves both vertically and horizontally with the stick-slip motion, and that the amount of the displacement at each point

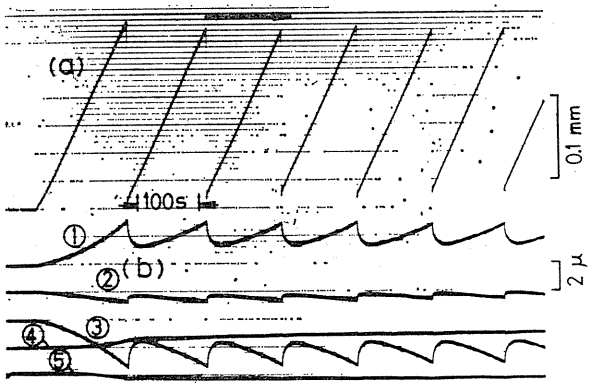

$v=0.12$ mm/min, Lubricant A, Driving position C_2.

Fig. 44. Experimental record of stick-slip motion and pitching and yawing motion.

varies with the same period as that of the stick-slip motion.

In an actual machine tool, such a pitching and yawing motion is transferred to the shape of the machined work, and in particular the periodic variation of the motion causes a deterioration of the machining accuracy directly and indirectly. Since this pitching and yawing motion may be closely related to the stick-slip motion, the characteristics of the stick-slip motion are first investigated for different driving conditions as shown in Fig. 42.

Figures 45 and 46 show the relation between the driving speed v and the amplitude a or the frequency f of the stick slip motion for different driving positions (see the points C_1, C_2, C_3, F in Fig. 42). It is seen in the figures that the amplitude a decreases abruptly from a large value as the driving speed v increases

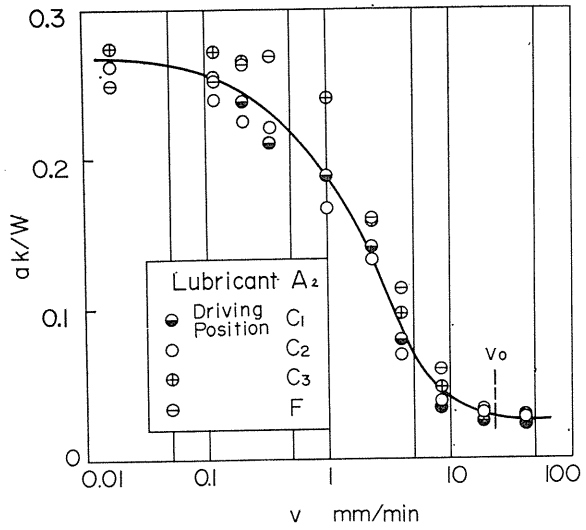

Fig. 45. Amplitude-driving speed curves.

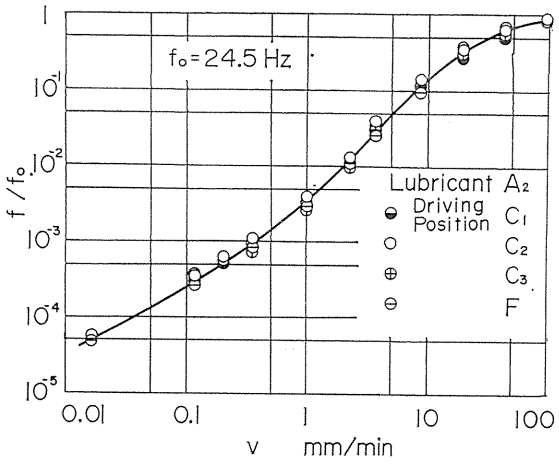

Fig. 46. Frequency-driving speed curves.

and beyond the speed v_0 the amplitude converges to a very small value, and that the frequency f increases almost proportionally to the driving speed and it converges to the value of the natural frequency f_0. However, it is evident in the figure that very little effect of the driving mechanism on the characteristics of the stick-slip motion is found under these experimental conditions.

The characteristics of the pitching and yawing motion of the slider accompanied by the stick-slip motion are studied here.

Figure 47 is a brief schematic diagram of the stick-slip motion and the pitching and yawing motion. In the figure, the curve (a) indicates the changing process of the spring force with the driving motion, and the curve (b) indicates the vertical

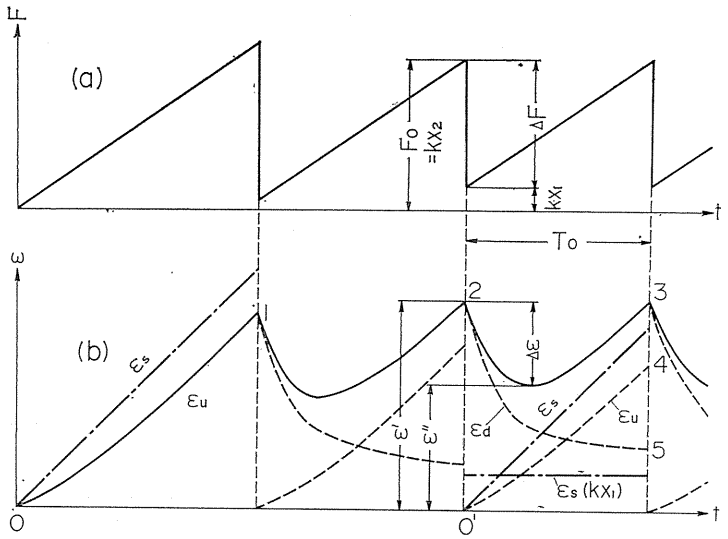

Fig. 47. Schematic diagram of pitching and yawing motion.

displacement in the pitching motion at a representative measuring point on the slider.

Figures 48 and 49 show the characteristics of the pitching ang yawing motion

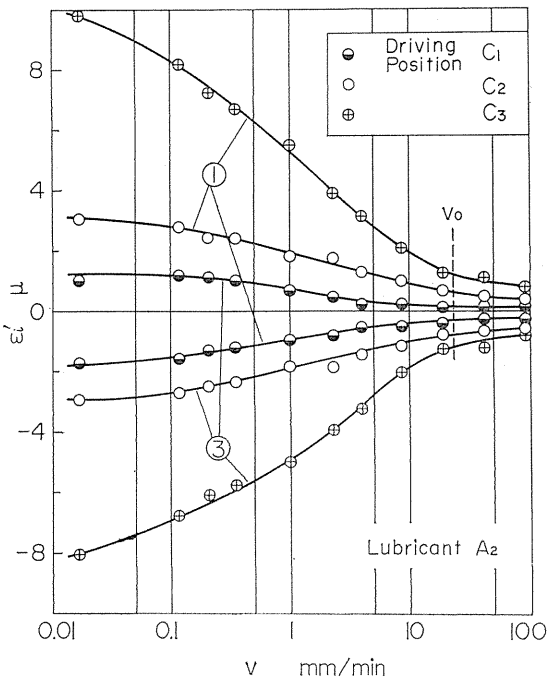

Fig. 48. Relation between driving speed and pitching motion.

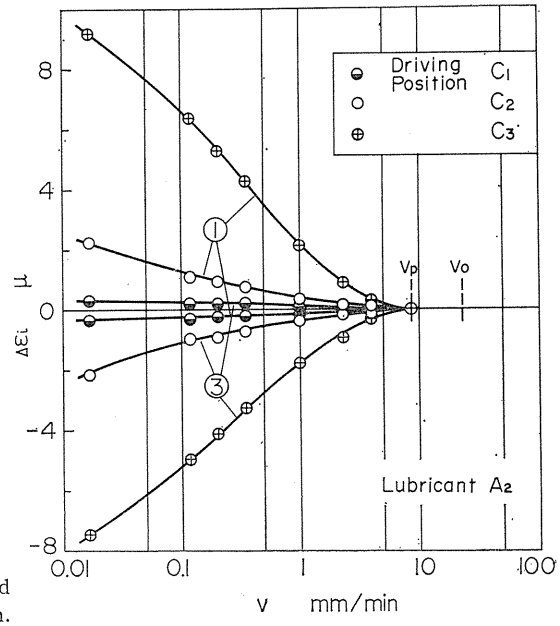

Fig. 49. Relation between driving speed and variation of pitching motion.

for various driving positions (see the points C_1, C_2, C_3 in Fig. 42). Figure 48 indicates the relation between the driving speed v and the maximum vertical displacement ε in the pitching motion. Figure 49 indicates the relation between v and the variation $\Delta\varepsilon$ of the vartical displacement (see Fig. 47). Since it is evident in the figure that the displacement of the point 2 (see Fig. 42) is much smaller than that of the poins 1 and 3 as seen in the experimental records of Fig. 44, in the following part of this chapter, the displacement of the points 1 and 3 is examined mainly when the pitching motion of the slider is discussed. It is considered that the relative amounts of the displacement of each point 1, 2, 3 are connected with the condition of the contact of the slideway, and that in this experiment the smallest displacement is found at the point 2 and at the diagonally opposite position to the point 2 which are near the points d and g (Fig. 42), where the intimate contact may be produced as seen from Fig. 43.

It is found from Fig. 48 that for the driving points C_2 and C_3, the measuring point 1 moves to the positive direction (up ward) and the point 3 moves to the negative direction (downward), and that the absolute values of the displacement of both the measuring points are nearly equal. Hence, it is recognized that the slider moves in a forwardly inclined posture to the sliding direction. For the driving point C_1, however, it is seen that the slider moves in a backwardly inclined posture, but the amount of the inclination is considerably small. It is concluded that for any driving point the value of ε' is fairly large in the region of small values of v, and that ε' becomes smaller with increase of v and it converges to a very small value beyond the speed as shown v_0 in the figure. The value v_0 corresponds to the speed beyond which the amplitude a of the stick-slip motion reaches a small value as shown in Fig. 45.

In regard to the effect of the driving mechanism, it is found that the characteristics of the pitching motion are influenced strongly by the position of the driving point in contrast to the fact that the characteristics of the stick-slip motion are influenced very little by it as shown in Fig. 45. That is, the value of ε is largest for the driving point C_3 which is the most distant point from the surface of the slideway, for the point C_2 the value of ε' is medium, and for the point C_1 which is the nearest point to the surface of the slideway ε is smallest.

It is found from Fig. 49 that in the region of small values of v, the variation $\Delta\varepsilon$ of the pitching motion is large and it almost equals to the value of ε', that the value of $\Delta\varepsilon$ decreases abruptly as v increases, and that the critical driving speed shown as v_p in the figure $\Delta\varepsilon$ becomes zero. It is recognized that the slider slides in the posture of constant inclination beyond the speed v_p.

Then, comparing Fig. 49 with Fig. 48, it is found that the critical value v_p is considerbly smaller than the value of v_0 at which the stick-slip motion disappears. Moreover, in regard to the effect of the driving mechanism on $\Delta\varepsilon$, the value of $\Delta\varepsilon$ generally increases as the vertical position of the driving point becomes higher, and such tendency is the same as that of shown in Fig. 48.

Figure 50 shows the relation $v\sim\varepsilon$, or $v\sim\Delta\varepsilon$ for different driving points which are changed in their horizontal positions (see the points V, C_2, F in Fig. 42). It is recognized from the figure that the horizontal position of the driving point has little influence on the value of ε and $\Delta\varepsilon$.

Figure 51 shows the relation $v\sim\varepsilon$ or $v\sim\Delta\varepsilon$ for various applied lubricants. It is found from the figure that both ε and $\Delta\varepsilon$ generally increase as v increases, but the

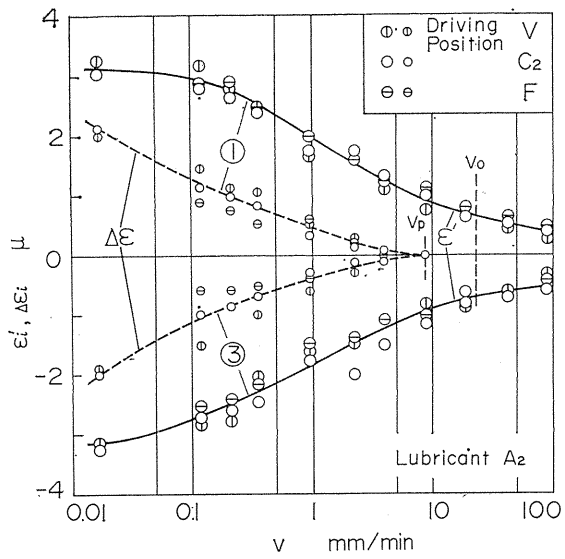

Fig. 50. Relation between driving speed and pitching motion.

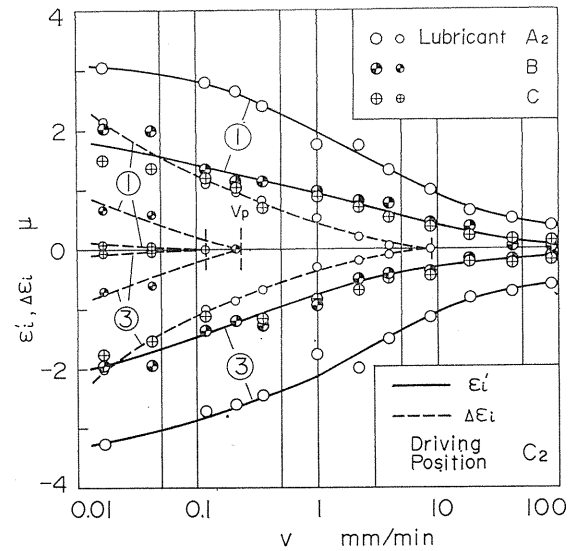

Fig. 51. Relation between driving speed and pitching motion.

magnitudes of ε and $\Delta\varepsilon$ and the decreasing tendecy of those with v are different considerably depending on the sort of applied lubricant. That is, the value of ε for the lubricants B and C are considerably smaller than those for the lubricant A_2, but the discrepancy between the values of ε for the lubricants B and C is not found clearly.

Meanwhile. in regard to $\Delta\varepsilon$, the value for the lubricant A_2 is largest, and the discrepancy between the values for the lubricants B and C is found to exist clearly.

Moreover, it is found that the critical driving speed v_p at which the variation $\Delta\varepsilon$ of the pitching motion reaches zero is influenced remakably by the sort of applied lubricant, and the value of v_p is large in the order of the lubricants C, B and A_2. It is concluded from Fig. 51 that the effect of the applied lubricant is more remarkable on $\Delta\varepsilon$ than on ε. In particular, the characteristics ef $\Delta\varepsilon$ are considered to be an important factor from the fact that the value of $\Delta\varepsilon$ seems to affect directly the machining accuracy.

Figures 52 and 53 show the relation between the height h of the driving point

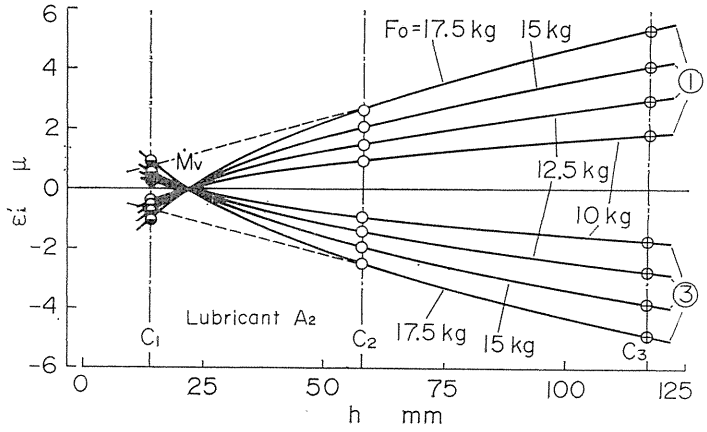

Fig. 52. Relation between vertical driving position and pitching motion.

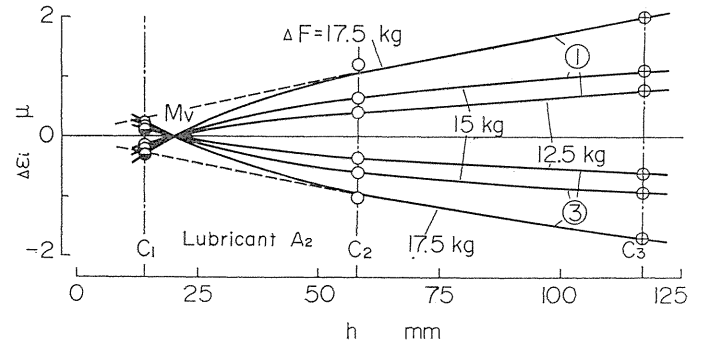

Fig. 53. Relation between vertical driving position and variation of pitching motion.

from the slideway and ε or $\Delta\varepsilon$ in order to make more clear the effect of the driving position on the characteristics of the pitching motion. In these figures, the maximum frictional force F_0 and the variation ΔF of the driving spring force in the stick-slip motion (see Fig. 47) are taken as parameters, respectively. From the figures, it is recognized that the value of ε and $\Delta\varepsilon$ generally increase as both values of h and F_0 or ΔF increase exept for the small value of h.

In an actual machine tool, usually there exists a certain distance between the

driving position and the acting position of the frictional resistance as in this experiment. A considarable magnitude of the rotating moment based on this distance seems to act on the slider, and this moment for the pitching motion seems to be proprtional to h and F_0. It is expected from the reltion shown in Fig. 52 that the amount of the pitching motion ε of the slider is determined mainly by the magnitude of this moment. Similarly, it is expected from Fig. 53 that the value of $\Delta\varepsilon$ is determined by the variation of the moment, too. But the magnitudes of ε' and $\Delta\varepsilon$ in the pitching motion originating from the rotating moment and its variation with v are considered to be affected by the sort of the applied lubricant as mentioned later. Moreover, it is seen from Figs. 52 and 53 that both ε and $\Delta\varepsilon$ lose their proportionalities to h in the region of small h and at the point Mv in the figures ε' and $\Delta\varepsilon$ are zero, and that for the drivng point C_1 the direction of the pitching motion is reverse to those for the driving points C_2 and C_3. This fact is considered to be connected with the correlation between the pitching motion of the slider accompanied by the stick-slip motion and the figure or the condition of the contact of the slideway. Since the rotating moment is very small for the driving point C_1, the pitching motion originating from this moment seems to be small. However, at the same time a slight horizontal dis placement of the slider occurs, and then near the measuring point 2, where the condition of the contact is intimate, the slider climbs up along of the inverted V part with that horizontal displacement. As a result, the slider has a little vertical component of displacement in the negative direction at the measuring point 1 and in the positive direction at the point 3. Such behaviour seems to be seen in the same way for the driving points C_2 and C_3, too, but it is considered that such an effect of the horizontal displacement on the vertical displacement can be more remarkable for the driving point C_1 where the magnitude of ε' is relatively small.

6. 3. Mechanism of Pitching Motion

In the previovs section, the characteristics of the pitching motion of the slider accompanied by the stick-slip motion are investigated. Next, the mechanism of the pitching motion is studied.

When a driving motion with a constant speed is applied to the slider which rests on the slideway as shown in Fig. 47, the driving spring force F increases at a constant rate until it reaches the maximum frictictional force F_0 of the slideway as shown in the curve (a), and at the same time, the slider moves vertically along 01 curve with the increse of the spring force. This vertical movement is considered to increase almost proportionally to the increasing driving spring force of the curve ε_s if the driving speed is very small and hence the driving spring force can be regarded as a static one, but in this experiment the magnitude of the vertical movement is generally smaller than the curve ε_s mainly owing to the viscosity of the applied lubricant and the vertical movement varies along the cvrve ε_u. It considered that the viscosity of lubricant produces squeeze phenomena and prevents the pitching and yawing motion of the slider in general, and that the amount of squeeze effect depends on the viscosity of the lubricant and the variation rate of the rotating moment. The magnitude of the difference between ε_s and ε_u which are mentioned above seems to be affected by the driving speed.

As soon as the driving spring force exceeds the value F_0, the slider slips and the spring force falls down to the value kx_1 in the figure almost instantly. As a result, the slider recovers its displacement as shown in Fig. 47. In this process,

owing to the disturbance of the lubricant viscosity primarily, the slider can not recover its displacement very rapidly, and in the mean time of the recovering process, the increasing tendency of the displacement with the rise of the driving spring force becomes prominent. Thus, the slider is considered to show the behaviour as 1-2 or 2-3. Such process as 1-2 or 2-3 can be regarded as the resultant of the recovering movement accompanied by the falling in the drivnig force with the slip motion and the increasing movement with the increase of the spring force in the stick period. That is, if the spring force falls bown by ΔF with the slip motion from F_0 to kx_1, and then, if the spring force is kept at the value kx_1 invariably, the displacement of the slider is expected to recover gradually along the curve ε_d shown as 2-5 and to approach a certain value ε_s (kx_1) which corresponds to the spring force kx_1 on the line ε_s. On the other hand, with increasing driving spring force the displacement of the slider increases as the curve ε_u shown in 0-4 in the same manner as 0-1. Accordingly, the practical process 2-3 of the displacement can be recognized as the resultant of the curves ε_u and ε_d. Both the curves ε_u and ε_d are generally affected by the viscosity of the lubricant, and in particular the curve ε_u depends on the driving speed, too.

Such a hypothesis on the mechanism of the pitching and yawing motion is considered to be confirmed by compering the experimental records of the pitching and yawing motion with the calculated results obtained from the resultant of both the experimental curves ε_u and ε_d.

Figure 54 and 55 show the relation between the spring force F and the increasing process ε_u of the pitching motion of the slider for different driving speeds and for different sort of the applied lubricant, respectively. It is found from the figures that ε_u decreases generally with the increase of the driving speed and increase of the viscosity of the lubricant. In both figures, the broken lines indicate ε_s which are obtained experimentally under the condition where the driving speed is very slow and the squeeze effect of the lubricant seems almost to disappear.

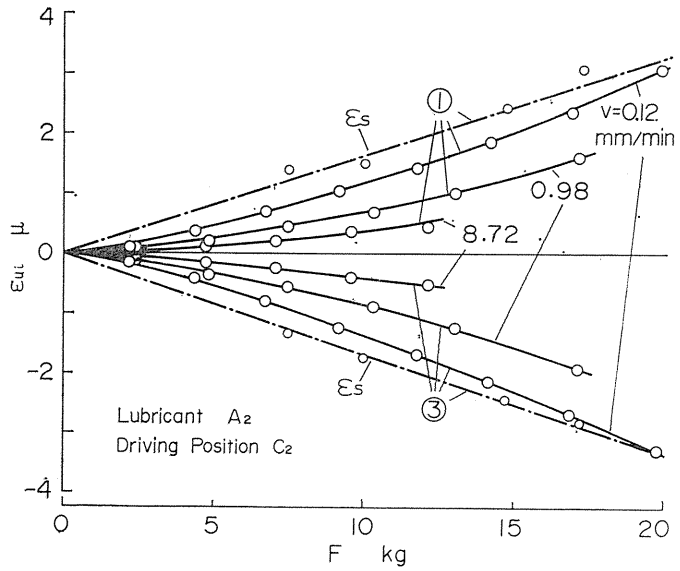

Fig. 54. Increasing process of pitching motion.

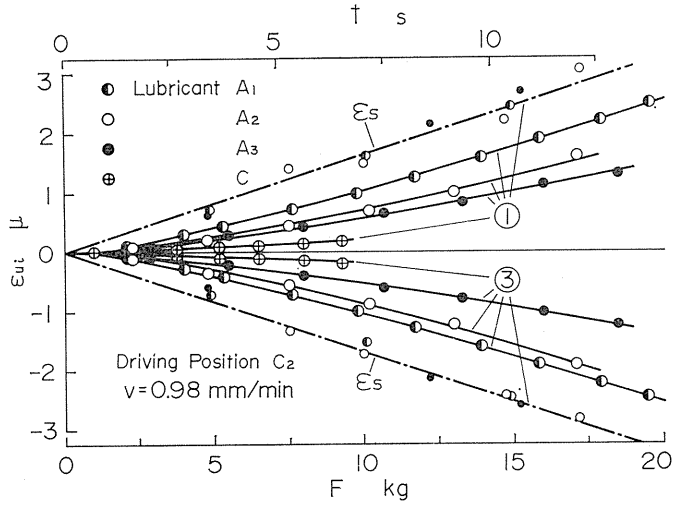

Fig. 55. Increasing process of pitching motion.

From Fig. 55, the lines ε_s are recognized to be almost independent of the sort of the applied lubricant.

Figure 56 shows some examples of the curve ε_d which indicates the recovering process of the pitching motion obtained experimentally to simulate the behaviour

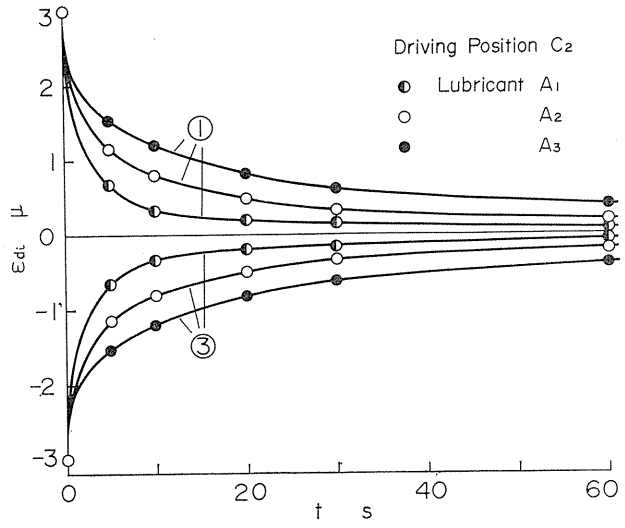

Fig. 56. Recovering process of pitching motion.

of the slider in the slip period by means of quick removal of the spring force from a certain value. It is found from the figure that it takes longer time for the recovery as the viscosity of the lubricant increases.

Figure 57 indicates an example of the comparison of the calculated result of the pitching motion obtained from the curve ε_u and ε_d as shown in Figs. 54-56

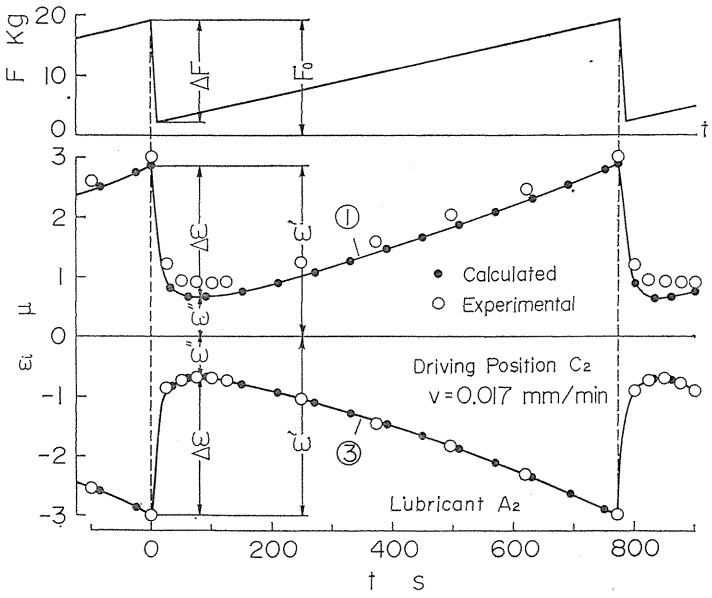

Fig. 57. Example of pitching motion obtained from calculation.

with the exprimental results at the measuring points 1 and 3 of the slider. It is recognized from the figure that the calculated results agree very well with the experimental results over the whole period of the stick-slip motion.

Figure 58 indicates the relation between v and ε' or $\Delta\varepsilon$ calculated by the above

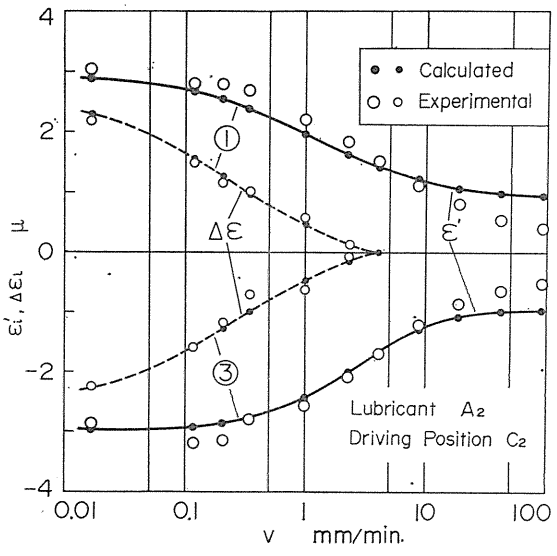

Fig. 58. Calculated pitching motion.

procedure, and the experimental results are shown at the same time. From the figure, it is found that the calculated results agree well with the experimental results for both ε' and $\Delta\varepsilon$.

Figure 59 shows the comparison of the calculated results which are obtained

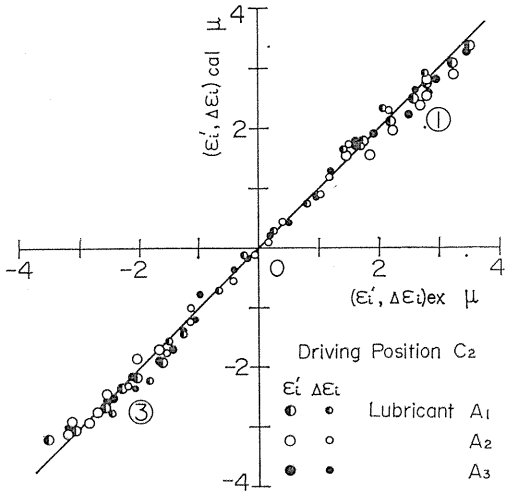

Fig. 59. Comparison between calculated and experimental results.

from many curves for the differnt conditions corresponding to Fig. 57 with the experimenal results for ε' and $\Delta\varepsilon$. It is found from the figure that over a wide range of ε' and $\Delta\varepsilon$ both the experimental and calculated results coincide with one another very well.

The propriety of the hypothesis, that the pitching motion of the slider with stick-slip motion may sppear as the resultant of the recovering moment accopanied by the falling in the driving spring force with the slip motion and the increasing movement with the increase of the spring force in the stick period, is confirmed from the above investigtions.

Thus, it becomes clear that the pitching motion can be calculated fairly accurately on the basis of the curves ε_u and ε_d obtained experimentally.

6. 4. Yawing Motion of Slider with Stick-Slip Motion

In the previous section, the characteristics of the pitching motion of the slider have been investigated.

The characteristics of the horizontal displacement, that is yawing motion, are studied here.

Figures 60 and 61 show the relations between the driving speed v and the maximum horizontal dispacement ε' or its variation $\Delta\varepsilon$ for various driving points F, C_2, V which are changed in horizontal position. The characteristics of the stick-slip motion are recognized to be almost identical between them as shown in Figs. 45 and 46. From Fig. 60, it is found that both points 4 and 5 move horizontally in counter direction to one another, and that with an increase of the driving speed v, the amount of such yawing motion ε decreases and beyond v_0, ε' becomes very small.

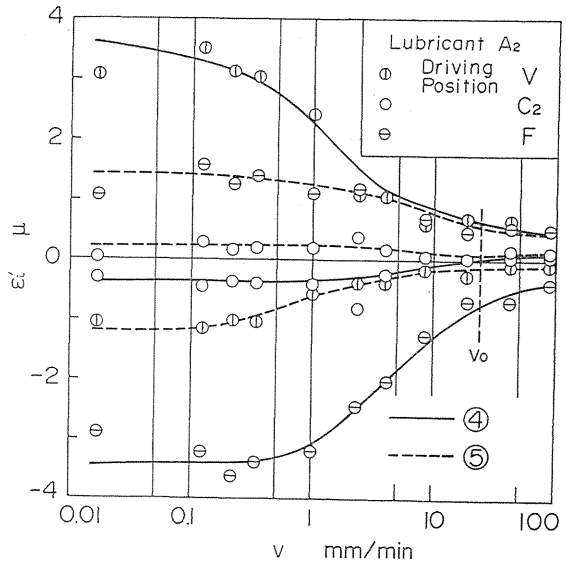

Fig. 60. Relation between driving speed and yawing motion.

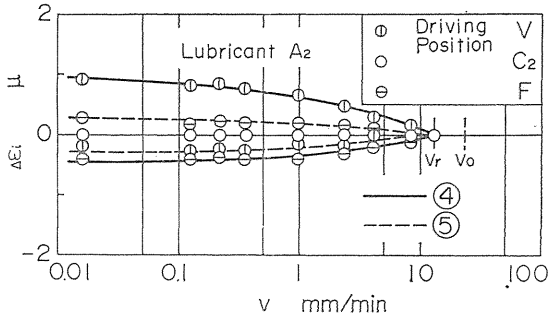

Fig. 61. Relation between driving speed and variation of yawing motion.

These $v \sim \varepsilon'$ characteristics of the yawing motion are almost identical with those of the pitching motion, but it is found that the direction and magnitude of the displacement are affected markedly by the horizontal position of the driving point.

From Fig. 61, it is seen that the value of $\Delta\varepsilon$ is much smaller than that of ε', or than that of $\Delta\varepsilon$ in the pitching motion, hence, the characterstics of the yawing motion are rather different from those of the pitching motion. This tendency is considered to depend on the fact that in the vertical direction the recovering moment for the pitching motion from the dead weight of the slider itself exists, but in the horizontal direction only a slight recoverhng moment from the horizontal reaction at the inverted V part of the slideway exists.

Figure 62 shows the relation between the value of l which is the distance from center of gravity of the slider to the driving point and ε' in order to make clear the dependence of the yawing motion on the horizontal plane. in the figure, $l=0$ indicates that the driving point is identical to the center of gravity of slider. It is found that the displacement ε' becomes zero at the point Mh in the figure which deviates slightly from that point ($l=0$ to the part V, and that at both sides of Mh

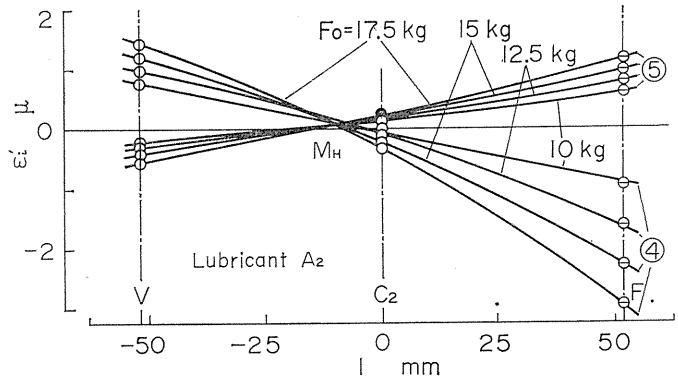

Fig. 62. Relation between horizontal position of driving point and yawing motion.

the direction of the displacement is contrary. Furthermore, it is recognized from the figure that ε' varies proportionally to l. Regarding the point Mh as an acting point of the frictional resistance in the horizontal plane, it is considered that the yawing motion depends on the moment in the horizontal plane which occurs from the frictional resistance and the driving force. The fact that the point Mh which is regarded as the acting point of the frictctional resistance differs from the center of gravity of the slider is due to the difference in the frictional resistance at each part of V and F of the slideway.

These characteristics of the yawing motion as well as those of the pitching motion seem to be affected by the viscosity of the applied lubricant and the yawing motion may have close relation to the contact condition of the slideway, too.

Figure 63 shows the characteristics of the pitching and yawing motion for the

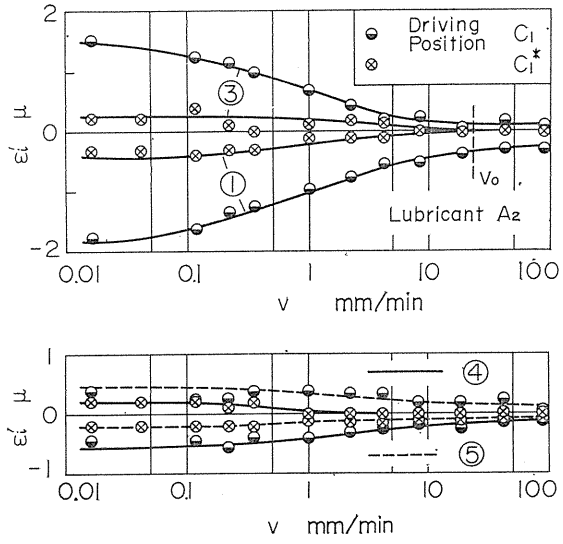

Fig. 63. Relation between driving speed and pitching and yawing motion.

driving point C_1* (see Fig. 42) the vertical position of which is equal to that of the point C_1, and the horizontal position of which is equal to that of the point Mh. For the driving point C_1*, the moment in the horizontal and vertical plane are minimum in this experiment. In this figure, (a) and (b) indicate the relations between the driving speed v and the vertical or horizontal displacement ε', respectively, and the value of ε' for the driving point C_1 is shown at the same time for reference. From the figure, it is recognized that the value of ε' for the driving point C_1* is much smaller than that for the driving point C_1. Then, it is clear that the pitching and yawing motion almost disappears if the driving point is placed at such position where the moment in the vertical and horizontal plane are minimum. Though this optimum driving position for pitching and yawing motion is affected by the figure of the slideway, the cutting resistance or other external force, there exists the optimum driving condition under a given sliding condition in the aspect of the pitching and yawing motion.

6. 5. Conlusion

It is clarified that the pitching and yawing motion is a phenomenon that the moving element slides with a slight inclination (ε') owing to the moment the caused by the driving force and the frictional resistance on the slide surfaces and amount of the inclination change ($\Delta\varepsilon$) with the stick-slip motion owing to the variation of the moment. It is concluded that the characteritics of the pitching and yawing motion are generally affected remarkably by the driving mechanism, the viscosity of the applied lubricant, etc.

7. Characteristics of Static Friction under Boundary Lubrication

On an actual machine tool slideway consisted of inverted V and flat surfaces and finished by sclaping, properties of stick slip motion was investigated as mentioned in Chapter 2. As results, it was clear that the friction of slideway especially static frictional characteristics dominate the properties of stick-slip motion.

In this chapter, mechanism of static friction under boundary lubricating condition is discussed.

7. 1. Experimental

Under boundary lubricating condition, it is considered that the characteristics of friction are controlled by contact condition of surfaces in micro scale and property of lubricant applied. In this experiment, in order to grasp precisely the contact condition and to replace easily with different suraces, model slideway with relatively simple shape and uniform surface topography is employed. But the dimension of slideway is not so small as compared with actual machine tool slideway.

7. 1. 1. Apparatus

Characteristics of static friction in stick-slip motion for a number of conbination of contacting surfaces and lubricants were investigated experimentally. The experimental apparatus consisted of four main sections as shown in Fig. 64; a slideway G, a slider S, a driving leaf spring k, and a driving device T.

The slideway had a pair of smooth guiderails R to drive the slider straight, and

was mounted on a rigid surface plate.

The slider consisted of a slide surface having varied surface topography, a projection B at which the slider was driven by the leaf spring, and four guide rollers arranged to cantact with the guiderails R. The projection B was set on a level with a slideway surface to prevent pitching and yawion of slider caused by stick-slip motion. The frictional force between guiderails and guiderollers was so much smaller than the frictional force between sliding surfaces that it could be considered negligible. Total weight of the slider was 12.4 kg in these experiments, and contact pressure was 0.344 kg/cm^2.

The relation between load and deflection of the driving leaf spring had a good linearity and its spring constant k=16.1 kg/mm. The approximate natural frequency of the spring was more than 800 Hz, and it was high enough compared to the stick-slip motion observed, so that the spring could completely follow the motion of the slider.

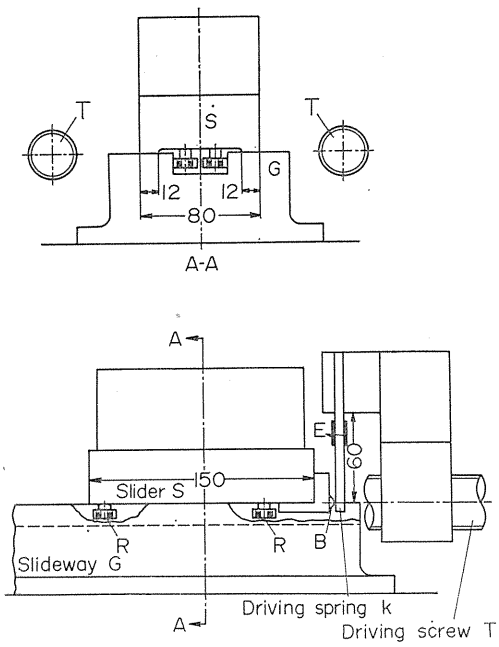

Fig. 64. Experimental apparatus.

The driving device was made from two accurate parallel ball screws with 5 mm pitch which were connected to one anether with a timing belt. The screw driven by a moter through a series of reduction gears. The gear combination permitted accurate control of driving speeds in the range from 0.004 to 80 mm/min.

7. 1. 2. Surface preparation

Five surface combinatios (S1G1-S5G5) were prepared for slider and slideway. Surfaces were all made of cast iron (Micro Vickers hardness number 200) and ground by cup type grinding wheel. The maximum height of asperities was in the range 0.5-20 μm. The surace had a flatness of 2 μm in the 300 mm length slideway. The surfaces ground by cup type grinding wheel is considered to be very convenient to study the frictional characteristics because such surface has no apparent directional effect. Figure 65 shows typical propfilographs of the sliding surfaces. These profilographs were obtained by stylus method, in which the radius of the stylus (4 μm) was much smaller than the radii of the suface asperities, so that the surface topography was measured precisely.

7. 1. 3. Lubricants

The lubricants employed in these experiments were seven commercially available oils. A description of the lubricants is given in Table 8. Heighly refined mineral oil A and the paraffin oil D do not contain any additives, while mineral oil B

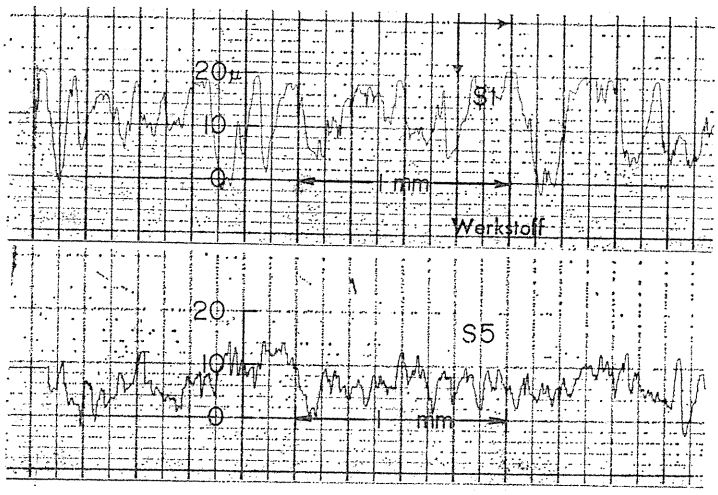

Fig. 65. Typical profilographs of sliding surfaces.

Table 8. Lubricants

Lubricants	Viscosity cSt at 20℃	Remarks
A	230.4	Naphthene base mineral oil
B	214.0	Commercial slideway lubricant
C	1108	Castor oil
D	212.4	Paraffin oil
E	86.4	Olive oil
F	514.8	Mixed oil (*C* 75%, *E* 25%)
G	266.0	Mixed oil (*C* 50%, *E* 50%)

contains various additives to meet the requirements of any type of sliding system. Castor oil *C* and olive oil *E* are both nondrying vegetable oils containing many types of chemically active species. Mixed oils *F* and *G* are a blend of caster oil and olive oil.

7. 1. 4. Test procedure

Experiments were carried out at constant room temperature (20+1 deg *C*) and with a uniform lubricating procedure. Initially the standard surface combination (S1 G1) was examined. After a thousand running in under lubrication, the surfaces were thoroughly cleaned with trichlorethylene prior to the actual experiment, and the test lubricant then applied to the surfaces. After a lapse of a day, the lubricant was wiped off and the test lubricant was supplied again. The slider was placed on the slideway and was run over the surface several times to remove exess lubricant from the surfaces and then experiments were run. The same procadure was employed for any test lubricant and also for any surface combination.

The deflection of the leaf spring x was measured by means of strain gauges

mounted on a spring and an electromagnetic oscillograph. *A* load versus deflection calibration of the spring permitted the translation of deflection into frictional force. The frictional force, the stick time, and the driving speed were mesured by tracings on the oscillogram.

The static frictional coefficient μ_0 was obtained by using the following equation,

$$\mu_0 = kx_2/W$$

where, x_2 = the maximum deflection of the driving spring (see Fig. 6).

7. 1. 5. *Experimental Results*

Figure 66 shows the exprimental static frictional coefficient μ_0 versus stick

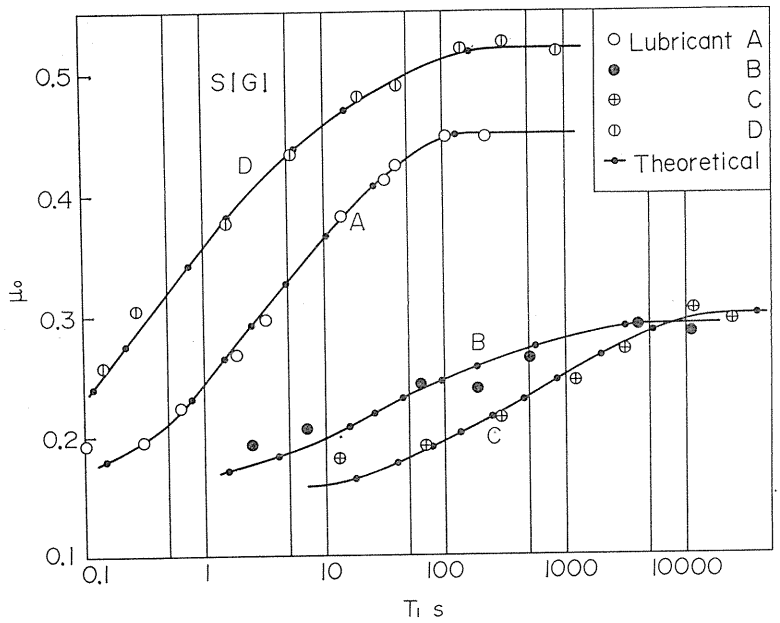

Fig. 66. Experimental and calculated $\mu_0 - T_1$ curves.

time T_1 curves for the standerd surface combination and various lubricants applied. In the figure, the time dependence of static friction similar to the results shown in section 3. 1 is found. In the same figure, solid curves show the results calculated by equation (1). In these cases, the value of the parameters μ_s, μ_d, γ and m for the various applied lubricants are summarized in Table 9. The calculated $\mu_0 \sim T_1$ curves show good agreement with experimental results in this experiment too, and the time dependence of static friction be well expresed by

Table 9. Chart of parameters

Lubricants	μ_s	μ_d	γ	m
A	0.450	0.156	0.286	0.671
B	0.290	0.160	0.211	0.362
C	0.300	0.150	0.0436	0.473
D	0.520	0.184	0.637	0.413

equation (1) for a wide range of stick time. In the following sections, the mechanism of the time dependence of static friction, and the physical meanings of the parameters involved in the formula are discussed in detail.

7. 2. Mechanism of the Time-Dependence of Static Friction

7. 2. 1. Contact between Sliding Surfaces under Boundary Lubrication

In order to investigate the mechanism of the time effect on static friction, it is necessary to study the contact process between sliding surfaces under boundary lubrication.

When lubricated metal surfaces are placed in contact under an applied load, the asperities of the surfaces are deformed to support the applied load. As a result of this deformation, the lubricant film is trapped between the two metal surfaces and subjected to very high pressure. The pressure, however, may not be uniform over the whole region of contact. In the regions where the pressure is relatively high, local breakdown of the lubricant film can occur and metallic adhesions may develop.

The mechanism of boundary lubrication is diagrammed in Fig.67, In this figure, the region of the metallic adhesion is shown as A, and the region where the lubri-

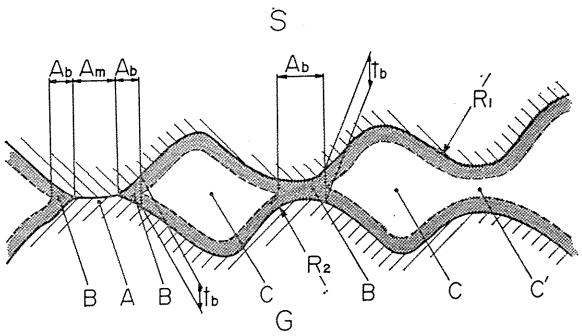

Fig. 67. Contact model under boundary lubrication.

cant surface film undergoes high pressure and carries a part of the applied load is shown as B, and the region where the liquid lubricant spreads over the microcavities between the contact surfaces is shown as C. The pressure of lubricant in the region C is generally low, but in the limited region C' (a part of region C), where the distance between the tips of the asperties distributed on the contact sufaces is very small, the pressure of lubricant might be rather high.

The total normal load W of the slider is supported by these three regions and be expressed as follows

$$W = W_m + W_b + W_s = pA_m + p_bA_b + W_s \tag{13}$$

where,

W_m, W_b, W_s = the loads carried in the regions A, B, and C, respectively.
p = mean pressure at region A and nearly to yield pressure p_m of materials.
p_b = yield pressure of lubricant surface film.
A_m, A_b = contact area in regions A and B, respectively.

The last term in equation (13) W_s is the load-carrying force produced by the hydrodynamic effect of the liquid lubricant in the region C (especially in C') when the two surfaces approach each other. The hydrodynamic effect is considered to decrease with increase in stick time and W_s tends to 0.

Assuming that the sliding resistance of the liquid lubricant in C can be negligible because the resistance force in this region is generally smaller than that in the regions A and B, the frictional force F is nearly equal to the tangential force required to shear both regions A and B. Let the shear strength of two regions S_m and S_b be, respectively,

$$F=S_mA_m+S_bA_b \tag{14}$$

The static frictional coefficient μ_0 can be expressed as follows

$$\mu_0=\frac{S_mA_m+S_bA_b}{p_mA_m+p_bA_b+W_s} \tag{15}$$

Consequently, it is considered that the time dependence of static friction may be caused by the decrease of W_s with increase in stick time and that the amount of A_m and A_b varies with the lapse of stick time.

Now, in order to examine the amount of A_m, A_b, and W_s, the mechanism of contact between surfaces must be studied.

7. 2. 2. Contact Area

A metal surface is generally composed of a large number of asperities. If each asperity is arranged in the order of its height, a certain distribution between the height and number of asperities can be obtained. Archard[15] assumed that the shape of surface asperity is hemispherical and that asperities are evenly disributde in depth over a surface. A more reasonable surface geometry is that of Fig. 68.

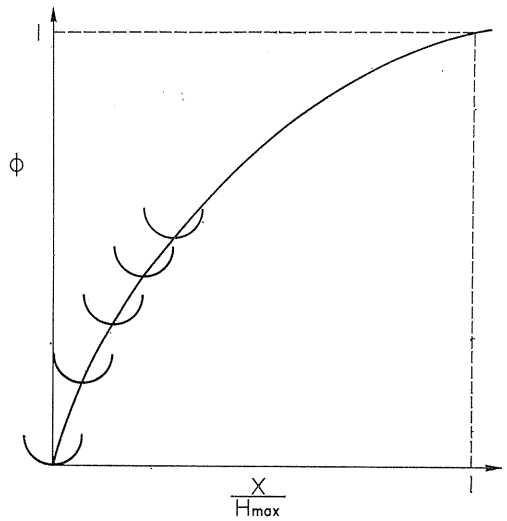

Fig. 68. Distribution function.

Now, let an ideally smooth surface be put a rough one and be deformed by an amount x from the top of the highest asperity; then let the ratio ϕ of the number of the contacting asperities I to the total number of the aspeerities I_0, be a distribution function. The function ϕ is generally expressed as folllows

$$\phi(x)=\frac{I}{I_0}=f\left(\frac{x}{H_{max}}\right)=D\left(\frac{x}{H_{max}}\right)^m \tag{16}$$

where,

H_{max} = maximum height of asperities
x = deformation or relative approach of two surfaces
D = distribution factor
m = distribution power

Both constants D and m depend on the surface preparation or the surface finish.

Let us assume that small identical hemispheres of radius R are distributed in depth (the X direction) as shown in Fig. 67, and are placed in contact with a flat surface. Figure 69 shows that the surface asperities exist at each of the X coordinates; $X=0$, $h^{1/m}$, $(2h)^{1/m}$, $(3h)^{1/m}$, ... $(ih)^{1/m}$ ....., where $h \ll R$. Equation (16) is transformed as follows

$$I=\frac{x^m}{h} \tag{17}$$

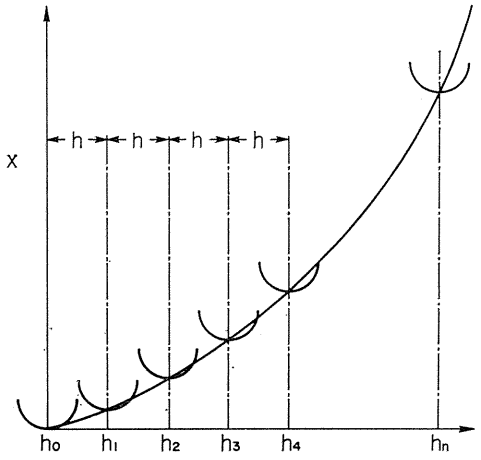

Fig. 69. Distribution of asperities in depth.

where,

$$h=(H_{max})^m/I_0D$$

When the rough surface deforms by amount x, the tip of the highest asperity (H_{max}) begins to contact and deforms by x, the deformation X_i of i th contacting asperity countered from the initial one is given as follows (cf. Fig. 70)

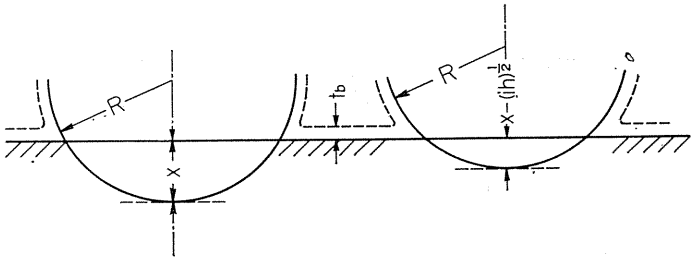

Fig. 70. Deformation of asperities.

$$Xi=x-(ih)^{\frac{1}{m}} \tag{18}$$

The contact area of i th contacting asperity δA_m is given by

$$\delta A_m=2\pi R\{x-(ih)^{\frac{1}{m}}\} \tag{19}$$

Hence, the total area of contact A_m may be obtained by summing up the contact area at each contacting point for large I and small h, as follows

$$A_m=2\pi R\int_0^I\{x-(ih)^{\frac{1}{m}}\}di \tag{20}$$

Here, assuming that each lubricant has an inherent value of the thickness of the lubricant surface film t_b adsorbed on a metal surface, the area A_b of the region B shown in Fig. 67 where a part of the applied load is supported by the adsorbed lubricant film, can be obtained by the same procedure. The annular contact area of i th contacting asperity with the lubricant film δA_b is given by

$$\delta A_b=\delta A_m(x+t_b)-\delta A_m(x) \tag{21}$$

Total contact area with lubricant film A_b is the sum of these areas.

$$A_b=A_m(x+t_b)-A_m(x) \tag{22}$$

The number of asperities in contact and the contact area of both rough surfaces can be obtained by extension of the results of contact between a rough surface and a flat surface.

The number of asperities in contact can be calculated from the contact model shown in Fig. 71 as proposed by kragelskii[16] who assumed that surface asperities consist of rods standing on a base plane. In this model, the base plane is extending out from the level of the lowest valley of surface asperities. This theory is very useful to study a contact problm in cases where the total number of asperies of each surace is very large and nearly equal to one another.

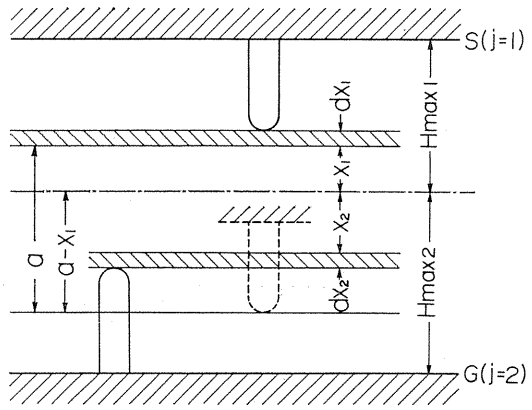

Fig. 71. Rod model of contacting surfaces from Kraghelsky.

If the surface j ($j=1, 2$) deformes by amount x relatively (cf.equation (16)), the number of asperities in contact I_j is given by

$$Ij=I_{0j}\phi_j(x_j) \tag{23}$$

The number of asperities with tips situated in layer dx_j at the distance from the tip of the highest asperity is given by differentiating equation (23)

$$dIj=I_{0j}\phi'_l(x_j)dx_j \tag{24}$$

In Fig. 71, the probability of contact between the tips of asperities in both layers dx_1, dx_2 is given by

$$\frac{dI_1}{I_{01}}\times\frac{dI_2}{I_{02}}$$

If the total number of asperities of both surfaces is nearly equal ($I_{01}\simeq I_{02}=I_0$), number of contacting asperities is given as a function of the relative approach of two surfaces a

$$I=I_0\int_0^a dx_1\int_0^{a-x_1}\phi'_1(x_1)\phi'_2(x_2)dx_2 \tag{25}$$

Equation (25) is transformed in the same form as equation (16)

$$\Phi=\frac{I}{I_0}=\int_0^a dx_1\int_0^{a-x_1}\phi'_1(x_1)\phi'_2(x_2)dx_2=\frac{a^m}{I_0h} \tag{26}$$

Equation (26) suggests that contact of rough surfaces with distribution functions ϕ_1, ϕ_2 can be equivalently translated to contact a rough surface with surface with distribution function Φ on a flat surface.

In order to calculate the contact area by the foregoing procedure, it is necessary that the contact of two spheres with curvatures R_1 and R_2 be replaced by the contact between an ideal flat surfacs with $R=\infty$ and a sphere with an equivalent curvature $R_e=(R_1R_2)/(R_1+R_2)$. Using the equivalent curvature, the contact areas A_m and A_b between rough surfaces can be obtained by the foregoing equations (20) and (22).

7. 2. 3. Hydrodynamic Effect of Lubricant

In Fig. 67, when two surfaces approach each other, the lubricant in the high pressure region (especially in region C', where clearance of asperities is very small) is gradually squeezed out to the low pressure region and hydrodynamic pressure is produced. This squeeze effect of lubricant contributes to carrying the load acting on the contact surfaces in transitional condition. The load carried by squeeze effect W_l is generally expressed as follows

$$W_l=-\frac{\eta Q}{h^3}\frac{dh}{dt} \tag{27}$$

where,

η = viscosity of lubricant
Q = squeeze factor
h = film thickness

The load carried by the microsqueeze effect of a lubricant under such boundary conditions as in these experiments cannot be expressed in the same form as equation (27). The load supported by the microsqueeze effect W_s under boundary lubrication as shown in Fig. 67 is given by replacing h in equation (27) with (h_e-t_b-a) as follows

$$W_s=\frac{\eta Q}{(h_e-t_b-a)}\frac{da}{dt} \tag{28}$$

where

h_e = effective initial film thickness
a = approach of two surfaces
da/dt = approaching rate of two surfaces

Equation (28) shows that W_s is proportional to the approaching rate and suggests that the time effect on μ_0 is due to the variation in the magnitude of W_s.

7. 2. 4. Analysis on the Time-Dependence of Static Friction

In a machine tool slideway, the deformation of asperities is much smaller the maximum height of asperity because in general the mean pressure w is relatively small. Hence, the distribution of the asperities in height can be approximated to a linear distribution (the distribution power $m=1$ in equation (16)), and expressed as follows

$$\phi_1(x_1)=D_1\left(\frac{x_1}{H_{max\,1}}\right) \qquad \phi_2(x_2)=D_2\left(\frac{x_2}{H_{max\,2}}\right) \tag{29}$$

The numqer of contact points I is given by equations (25) and (29).

$$I=\frac{I_0D_1D_2}{2H_{max\,1}H_{max\,2}}a^2 \tag{30}$$

The areas of contact A_m and A_b are given by equations (20), (22) and (30).

$$A_m=\frac{\pi R_eI_0D_1D_2}{3H_{max\,1}H_{max\,2}}a^3 \tag{31}$$

$$A_b=\frac{\pi R_eI_0D_1D_2}{3H_{max\,1}H_{max\,2}}\{(a+t_b)^3-a^3\} \tag{32}$$

For the standard surface combination S1G1, each factor involved in equations (30), (31), and (32) is obtained from the actual surface profilographs and given in Table 10. The thickness of adsorbed lubricant film t_b can be estimated as follows.

When the static friction μ_0 approaches the asymptotic value ($T_1\to\infty$), $F\to Fs$, $a\to a_s$, $h\to 0$ and the time effect on μ_0 disappears. Hence the last term in equation

Table 10. Test surfaces and their properties

Surfaces	Hmax mm	R mm	z 1/mm	D	ξ
$S1$	20.4×10^{-3}	21.4×10^{-3}	23.4	1.46	35.8
$G1$	19.6	16.6	23.9	1.57	31.8
$S2$	5.0	10.1	12.0	1.19	28.9
$G2$	7.2	12.0	11.3	0.81	16.6
$S3$	0.48	17.8	14.2	0.29	153
$G3$	0.46	14.4	14.4	0.38	173
$S4$	4.25	57.2	21.0	0.55	157
$G4$	4.66	46.9	16.0	0.71	115
$S5$	11.4	27.5	15.9	1.43	54.8
$G5$	12.4	25.3	14.1	1.43	41.4

(13) is negligible. The following equations are given referring (13) and (14).

$$W=p_mA_{ms}+p_bA_{bs} \tag{33}$$

$$F_s=S_mA_{ms}+S_bA_{bs} \tag{34}$$

where subscript s denotes the value corresponding to μ_s. Both values of t_b and a_s can be estimated from equations (31), (32), (33) and (34), where W is designated in this experiment and is obtained experimentally. The lubricant A, assuming that $S_m/p_m=1$, $p_b/p_m=1$, and $S_b/p_b=0.075$, respectively, following the data of many workers and average thickness of t_b, is estimated to be 0.211 microns.

For the standard surface combination S1G1 and the standard applied lubricant A, Fig. 72 shows A_m/A_0, A_b/A_0, (A_0 : apparent area of contact) I/I_0, μ_0, versus

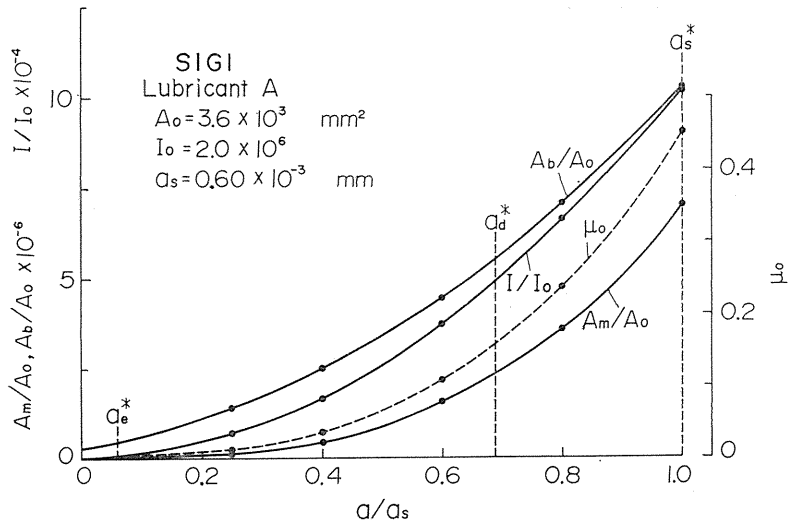

Fig. 72. A_m/A_0, A_b/A_0, I/I_0, μ_0-a/a_s curves.

a/a_s curves calculated from the equations described in the foregoing by applying each value shown in Tables 10 and 11. In the figure, a_d denotes the approach of

Table 11. Calculation chart of parameters

Lubricants	μ_s	μ_d	$\eta\times10^{-8}$ kg·s/mm²	$t_e\times10^{-3}$ mm	$h_e\times10^{-3}$ mm	Q mm⁴
A	0.450	0.156	2.2	0.211	0.851	28.4
B	0.290	0.160	2.0	0.312	0.826	47.6
C	0.300	0.150	9.79	0.305	0.831	150
D	0.520	0.184	1.90	0.176	0.821	5.25
E	0.252	0.161	0.800	0.344	0.825	16.5
F	0.297	0.192	4.99	0.308	0.830	75.0
G	0.300	0.176	2.54	0.305	0.830	35.0

two surfaces when $\mu_0\to\mu_d$, $T_1\to0$, and a_e is the maximum elastic deformation of asperities estimated from Hertz's equation. and a_e*, a_d*, and a_s* denote the dimensionless forms of a_e/a_s, a_d/a_s, and a_s/a_s, respetively. It is seen in the figure that I, A_m, and A_b increases as a increases, and as a result μ_0 increases.

Figure 73 shows the load carrying rate, W_m/W, W_b/W, and W_s/W versus deformation a/a_s curves for the conbination S1G1 and the lubricant *A*. Here, W_s is

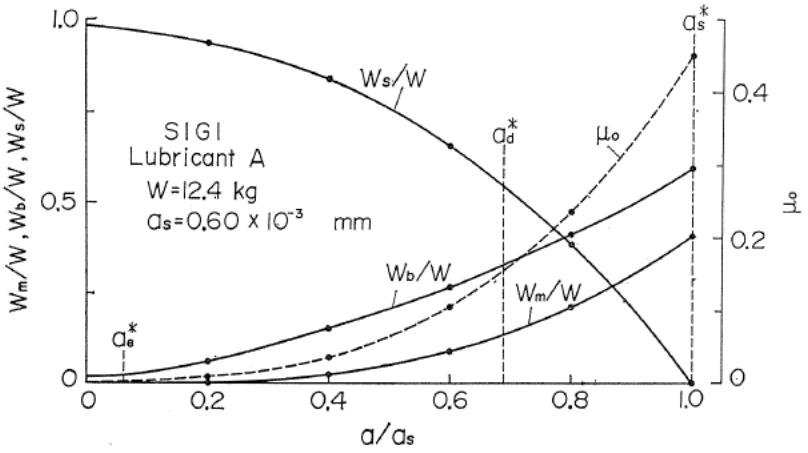

Fig. 73. Load carrying rate, W_n/W, W_b/W, $W_s/W-a/a_s$ curves.

calculated from equation (13) :

$$W_s=W-(W_m+W_b)$$

It is seen in the figure that W_s decreases gradually as a increases. Integrating equation (28) graphically using the W_s versus a curve shown in Fig. 73, the relation between a and T_1 can be obtained. As a result, the $\mu_0\sim T_1$ relation can also be

obtained. Consequently it becomes clear theoretically that static friction increases as stick time increases and approaches an asymptotic value.

The values of two parameters h_e and Q involved in equation (28) are considered to depend primarily on the topography of the contacting surfaces and the properties of the applied lubricant. However, they cannot be obtained by a direct measurement and have not yet been treated because the mechanism of microsqueeze effect under boundary lubrication is very complicated, and the analysis of microsqueeze phenomena is considered to be very difficult. Figures 74 and 75 show the influecnes of h_e and

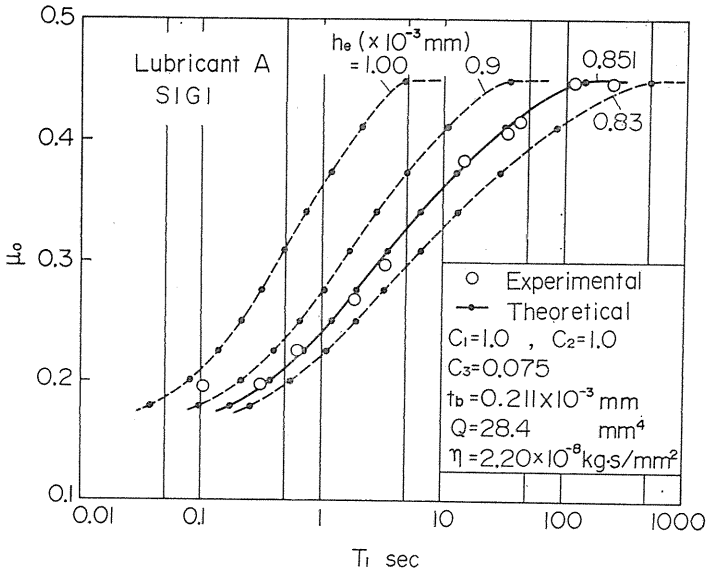

Fig. 74. Theoretical $\mu_0 - T_1$ curves.

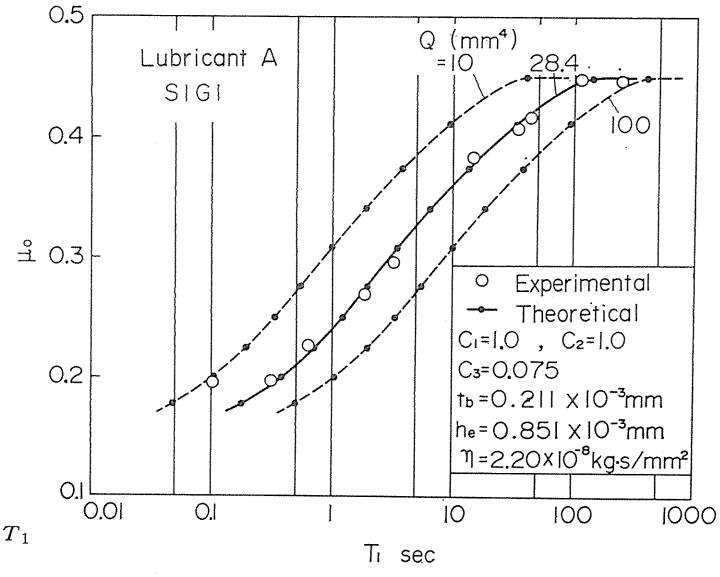

Fig. 75. Theoretical $\mu_0 - T_1$ curves.

Q on $\mu_0 \sim T_1$ curves, assuming the values of h_e and Q so that the $\mu_0 \sim T_1$ relation obtained theoretically almost agrees with the experimental results. It is seen in these figures that the trend of $\mu_0 \sim T_1$ curves depends greatly on the values of h_e and Q, and that h_e determines the amount of stick time reqired for μ_0 to reach the asymptotic value.

Figure 76 shows the $\mu_0 \sim T_1$ relation obtained theoretically by assuming the

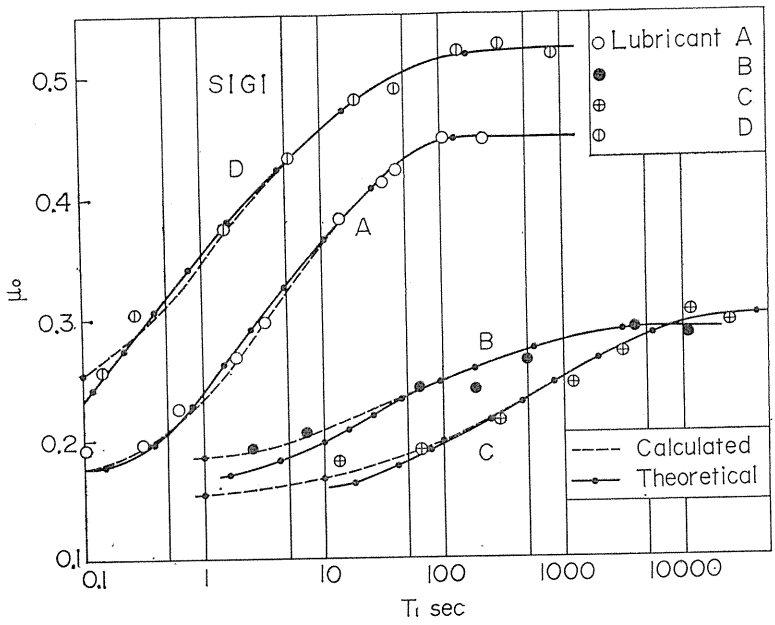

Fig. 76. Theoretical and calculated $\mu_0 - T_1$ curves for various lubricants.

suitable values of h_e and Q as seen from Figs. 74 and 75. and shows the comparison with that calculated from the authors empirical formula equation (1). It is seen in the figure that the theoretical results agree well with the experimental results.

In order to investigate the influence of the properties of the lubricant and the surface topography on h_e and Q, many experiments are carried out to obtain the $\mu_0 \sim T_1$ curves for many surface combinations and various applied lubricants. on the basis of the results, the correlation between h_e or Q and properties of lubricant or surface topography are obtained experimentally. The $\mu_0 \sim T_1$ curves ean be calculated theoretically on the basis of these correlations for any lubricant and any surface combination. From the foregoing procedure, the influence of the properties of lubricant and surface topography on the parameters γ and m involved in the empilical formula equation (1) can be clarified and be discussed in the following section in detail.

7. 3. *Influence of Lubricant on the Time-Dependence of Static Friction*

In this section, first, the relation between the properties of the lubricant and value of factors in equation (28) Q, h_e is investigated experimentally. Second, the

influence of properties of lubricant on the parameters γ and m involved in equation (1) is studied on the basis of the experimental results.

Figures 77 and 78 show the comparison between the experimental $\mu_0 \sim T_1$ curves and the theoretical ones obtained by using the values as shown in Tabe 11 for

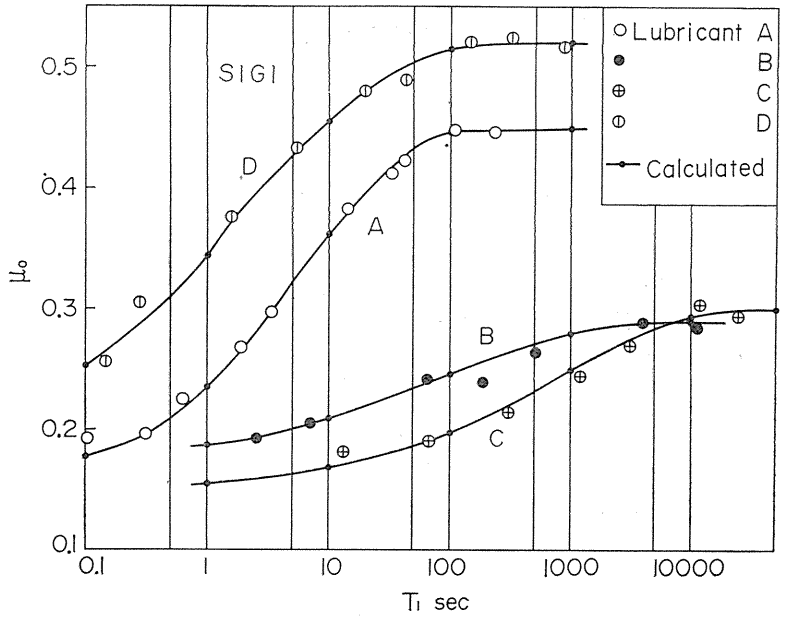

Fig. 77. Theoretical $\mu_0 - T_1$ curves for various lubricants.

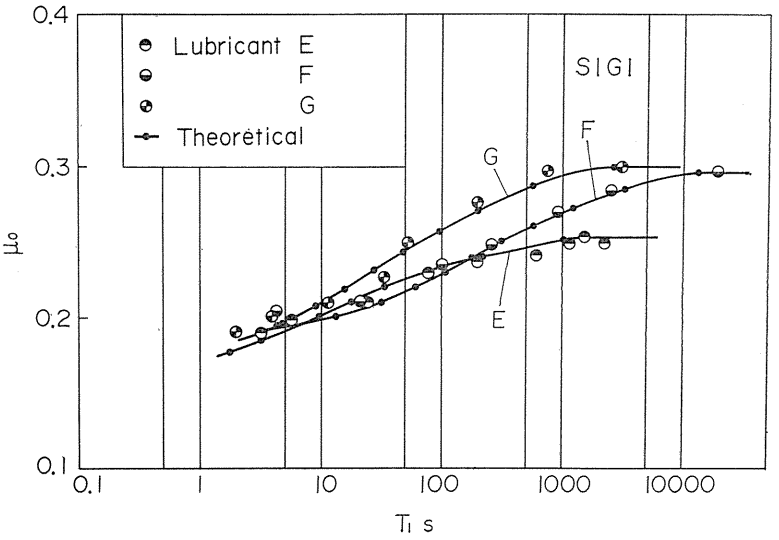

Fig. 78. Theoretical $\mu_0 - T_1$ curves for various lubricants.

various applied lubricants. The theoretical $\mu_0 \sim T_1$ curves agree well with the experimental results in the figures. Based on these figures, the correlation between the squeeze factor Q and the viscosity of the lubricant η for various surface combinations is obtained as shown in Fig. 79. It is seen in the figure that Q increases

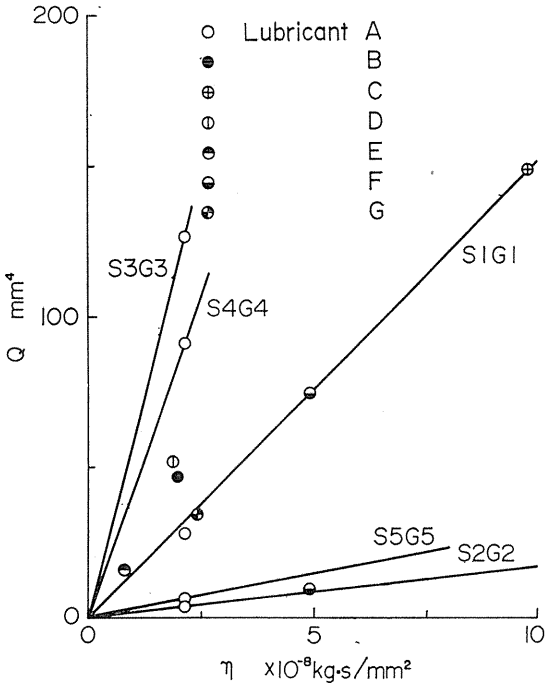

Fig. 79. Correlation between Q and η.

linearly with η and the increasing rate of Q with η depends remarkably on the surface topography. Regarding the $\mu_0 \sim T_1$ curves for homologous oils C, F, and G with various viscosity, it is recognized in Figs. 77 and 78 that the $\mu_0 \sim T_1$ curves lie to the right on the figures in the order of their viscosity while the values of μ_s for these oils are nearly equal. These results suggest that the time effect on static friction may be slight for a lubricant with high viscosity.

Figure 80 shows the relation between the effective initial film thickness h_e and the viscosity of lubricant η. It is seen in the figure that the value of h_e is not influenced by the viscosity of lubricant η but depends markedly on the surface topography. The value of h_e is connected with the initial average effective clearance between the asperities of contact surfaces approaching one another, and is nearly equal to the sum of the maximum deformation of the asperities a_s and the thickness of adsorbed lubricant film t_b. This is because when the slider is set on the slideway at rest for a long time, $T_1 \to \infty$ the lubricant between the asprities of contacting suraces is squeezed out and the equivalent squeeze film thickness h is nearly equal to zero, and then $h_e \simeq a_s + t_b$. The value of a_s is generally considered to be greater than the value of t_b, and the difference of the value of t_b for each

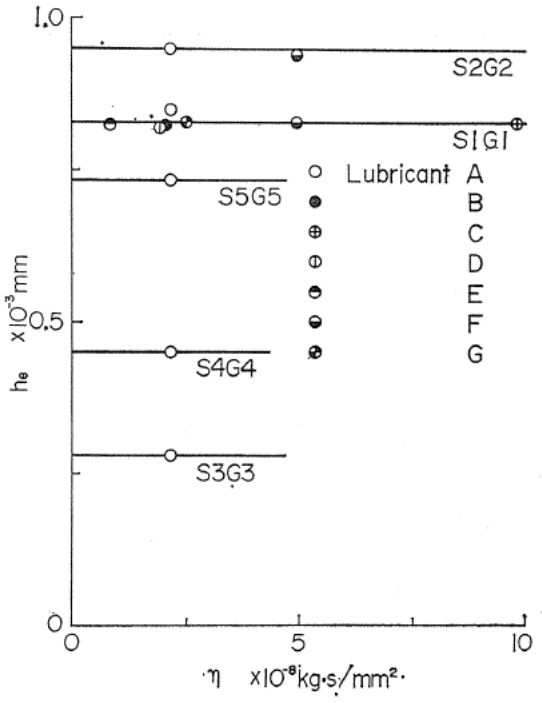

Fig. 80. Relation between h_e and η.

lubricant is small as seen in Table 11. Consequently, the value of h_e is closely related to the surface topography because a_s depends on that.

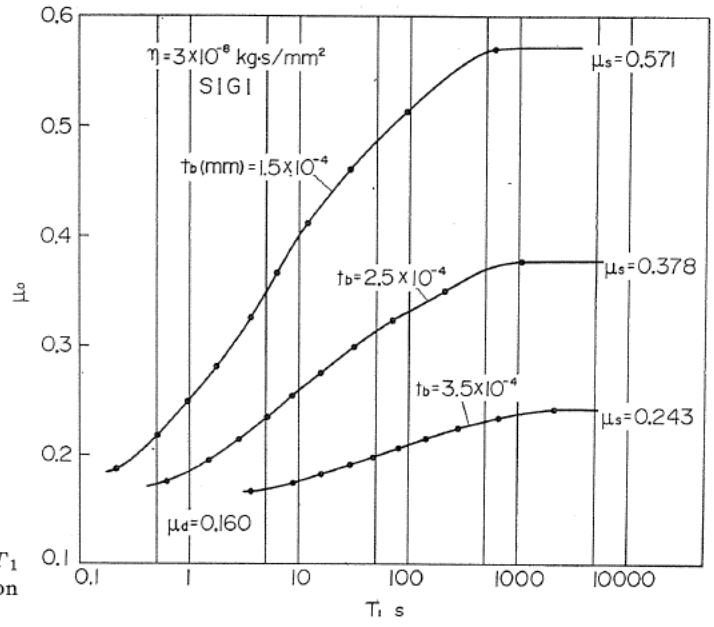

Fig. 81. Theoretical μ_0-T_1 curves as function of t_b.

The theoretical $\mu_0 \sim T_1$ curves can be obtained by the theory described in the previous section on the basis of the results shown in Figs. 79 and 80 where t_b and η are varied. Figure 81 shows an example of theoretical $\mu_0 \sim T_1$ curves for various values of t_b. In this calculation, the values of Q and h_e are determined from Figs. 79 and 80 as follows. $Q=46\,\mathrm{mm}^4$, $h_e=0.83\times10^{-3}\mathrm{mm}$ for $\eta=3\times10^{-8}\mathrm{kg\cdot s/mm}^2$. It is seen in the figure that the greater the value of t_b is, the smaller μ_0 and μ_s are. Applying the empirical formula equation (1) to theoretical $\mu_0 \sim T_1$ curves, the relation between the parameter μ_s, γ, and m involved in equation (1) and t_b can be obtained, and the influence of the thickness of the adsorbed lubricant film t_b on the time-dependence of static friction can be quantitatively examined.

Figure 82 shows the μ_s γ, and m versus t_b curves obtained by the foregoing procedure. It is seen in this figure that μ_s and γ depend heavily on t_b and decrease

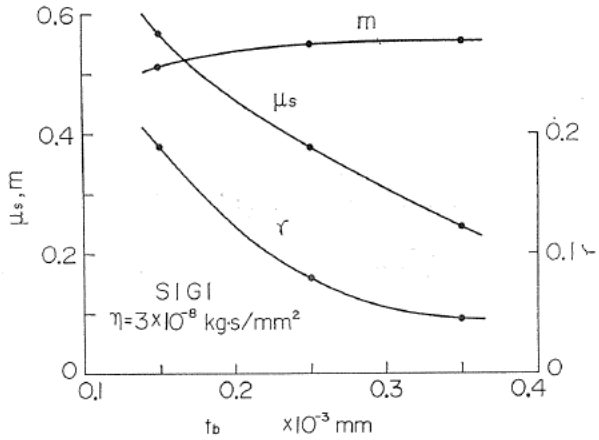

Fig. 82. μ_s, γ, and m versus t_b curves.

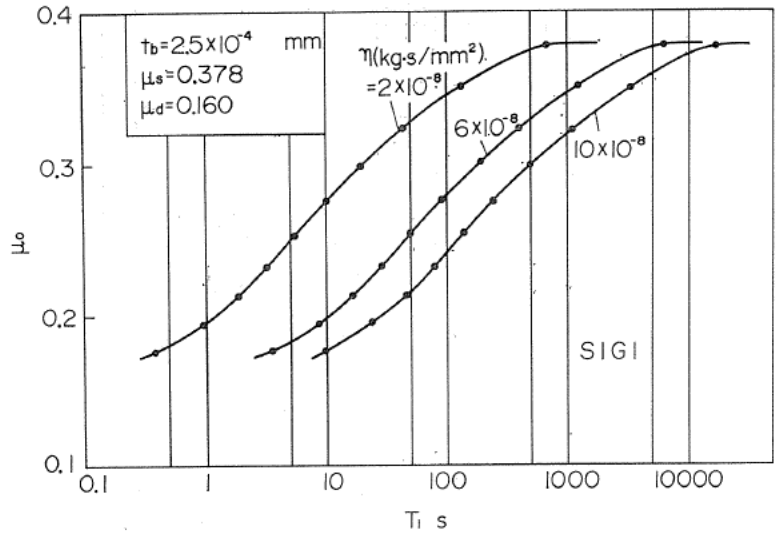

Fig. 83. Theoretical $\mu_0 - T_1$ curves as function of η.

as t_b increases, and also that m depends slightly on t_b and increases a little with increasing t_b.

Figure 83 shows the theoretical $\mu_0 \sim T_1$ curves for several lubricats having various viscosities in the same way as Fig. 82. The figure is for the standard combination S1G1, where h_e and Q are determined from Figs. 79 and 80, respctively, as follows: $h_e = 0.83 \times 10^{-3}$mm for S1G1, $Q = 31\,\text{mm}^4$ for $\eta = 2 \times 10^{-8}$kg·s/mm^2, $Q = 92\,\text{mm}^4$ for $\eta = 6 \times 10^{-8}$kg·s/mm^2 and $Q = 153\,\text{mm}^4$ for $\eta = 10 \times 10^{-8}$kg·s/m^2. It is seen that the higher viscosity η is the longer the stick time required for μ_0 to reach the asymptotic value; but the asymptotic value μ_s is not influenced by the viscosity η because a constant t_b is assumed.

Figure 84 shows the μ, γ, and m versus η curves obtained by the same procedure as Fig. 82 on the basis of the theoretical $\mu_0 \sim T_1$ curves shown in Fig. 83. It

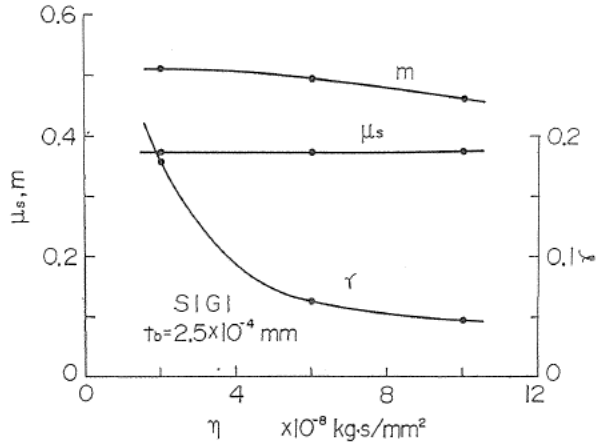

Fig. 84. μ_s, γ, and m curves.

is recognized in the figure that μ_s does not depend on η and that γ is rather affected by η. It decreases with increasing η and its decreasing rate varies with η, and moreover m depends slightly on η, decreasing as η increases.

From the results described in the foregoing, it is concluded certainly that the time-dependence of the static friction of machine tool slideway depends markedly on the properties of the applied lubricant for each surface combination, and it can be evaluated by specific value of lubricants μ_s, γ, and m which are closely correlated with the adsorbed lubricant film thickness t_b and the lubricant viscosity η,

7. 4. Influence of Surface Topography on the Time-Dependence of Static Friction

In order to investigate the relation between the frictional behaviour and the surface topography, problems of how to estimate the surface topography concretely and entirely are significant. In this section, the influence of size, shape, and distribution of asperities on the time-dependence of static friction is first investigated theoretically. A new numerical parameter is proposed to describe the surface topography entirely. Then, the relation between this new nunnerical parameter, and μ_s, γ, and m involved in equation (1) is investigated.

Based on the contact mechanism described in section 7. 2, the surface topography may be estimated by the following factors; the maximum height of asperities H_{max}, the shape of the asperity (if the shape of asperity is assumed to be hemispherical, the curvature R), the number of asperities per unit length of the surface Z which gives the density of the asperities distributed over the surface, the distribution factor of asperities in height (if the asperities are assumed to distribute linearly in height, distribution factor D). Then, the influence of these factors on the characteristics of static friction, especially μ_s, is investigated theoretically.

In the calculation of μ_s, the following factors are assumed; H_{max1}, $H_{max2}=20\,\mu$; R_1, $R_2=20\,\mu$; D_1, $D_2=1.5$; $z=251/\text{mm}$; and t_b is determined as $t_b=0.2\,\mu$. These values nearly correspond to the values for the standard surface combination S1G1 and the standard subricant A applied in this experiment. Assuming that three factors among them are assigned and the other one is variable, μ_s can be calculated by using equations (31), (32), and (33) and the following equation (35) derived from equation (34). When $Ws=0$, A_{ms} and A_{bs} are obtained as follows

$$A_{ms}=\frac{W}{p_m}\frac{C_3-\mu_s}{C_3-C_1}$$
$$A_{bs}=\frac{W}{p_m}\frac{\mu_s-C_1}{C_2(C_3-C_1)} \tag{35}$$

where,

$W=12.4\,\text{kg}$, $pm=200\,\text{kg/mm}^2$, $C_1=Sm/pm=1$

$C_2=p_b/p_m=1$, $C_3=s_b/p_b=0.075$

Figures 85, 86, 87, and 88 show the calculated $\mu_0\sim H_{max}$, $\mu_s\sim R$, $\mu\sim D$, and $\mu_s\sim z$ curves. It is recognized that the value of μ_s is greatly affected by these

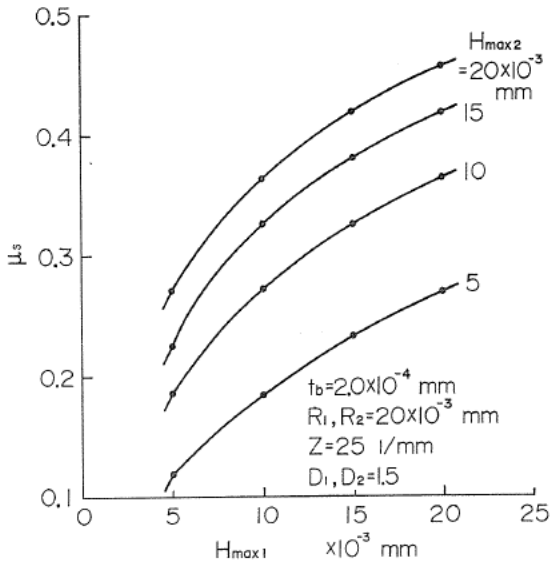

Fig. 85. Calculated μ_s-H_{max} curves.

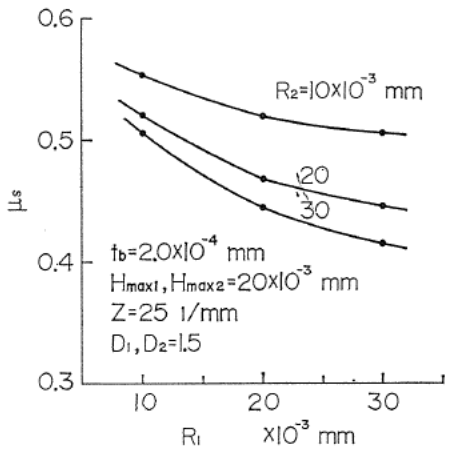

Fig. Calculated μ_s-R curves.

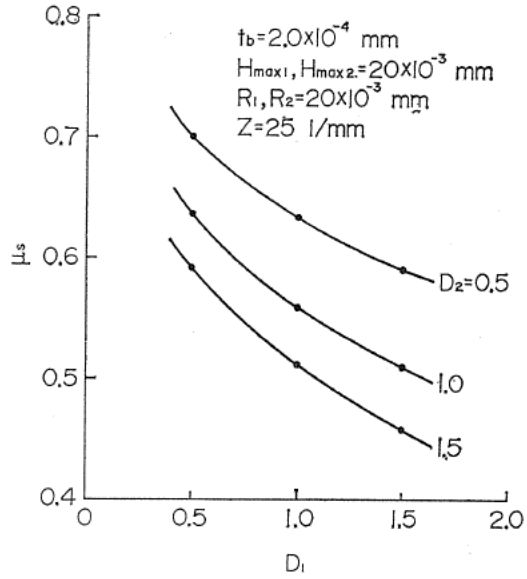

Fig. 87. Calculated μ_s-D curves

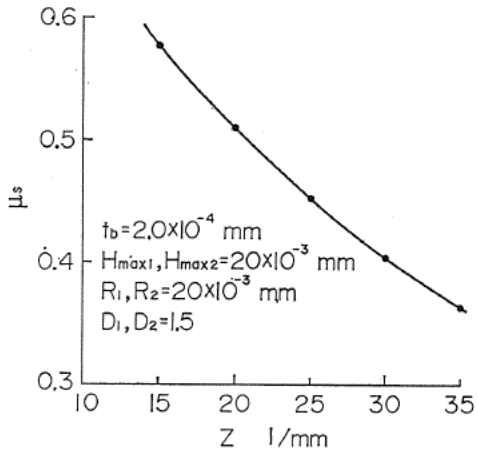

Fig. 88. Calculated μ_s-z curves.

factors. It is true that the larger H_{max} is and the smaller R, z, and D_1 are, the higher μ_s is. Here, small D means that few asperities distribute near the maximum height of asperities. These results coincide well with the general fact that the frictional coefficient becomes high under conditions where the lubricant film breaks down easily and metallic junctions are produced. Accordingly, it is concluded that the characteristics of static friction can be evaluated by the previously described factors.

In reference to equation (31) and (32), a nondimensional numerical parameter $\xi=D(R/H_{max})zL_u$ is proposed to estimate the surface topography where L_u is unit

length. The parameter ξ is called coefficient of surface topoqraphy in this research. A surface having a large value of ξ may be a good surface for friction and wear because it has a large bearing area near the maximum height of asperities. When two surfaces evalueted by ξ_1, ξ_2 are in contact, the effect of contact may be approximately estimated by the product $\xi_1\xi_2$. The relation between the characteristics of static friction and surface topography is discussed by using this new parameter.

Figure 89 and 90 show the distribution function of asperities for various surfaces of slider and slideway. If the distribution function is approximated to be

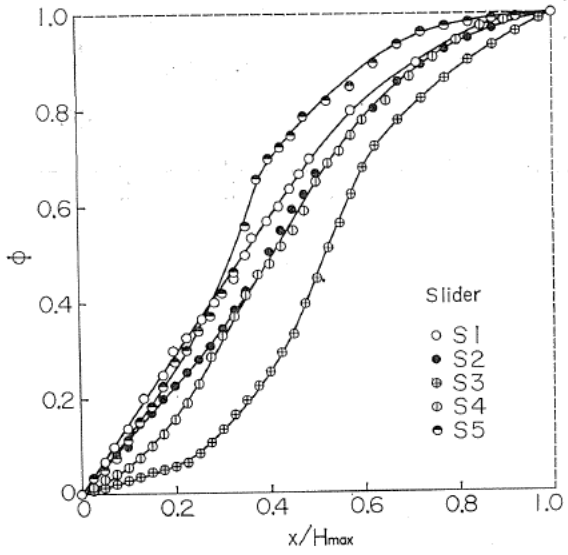

Fig. 89. Distribution function for slider.

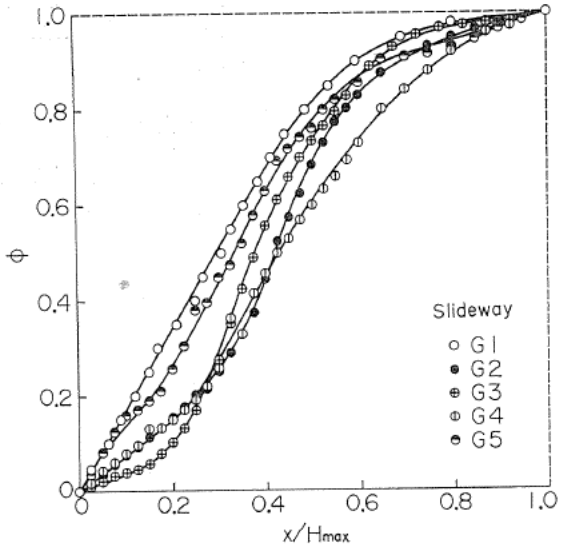

Fig. 90. Distribution function for slideway.

linear the maximum height of asperities, the distribution factor D is obtained from the inclination of the tangent line for each curve in the vicinity $x=0$. The values of H_{max}, R, z, D, and ξ for various surfaces are summarized in Table 10. The mean curvature of the asperities is determined as follows; the profilogram shown in Fig. 65 is magnified by an optical projector, and each asperity is intersected at a very small distance x from its tip, while the resulting width y of the cross section is measured accurately, and then the curvature determined by the relation $R \simeq y^2/8x$.

Figure 91 shows the comparison between the experimental results and the theoretical $\mu_0 \sim T_1$ curves for five surface combinations I, II, III, IV, V, where the

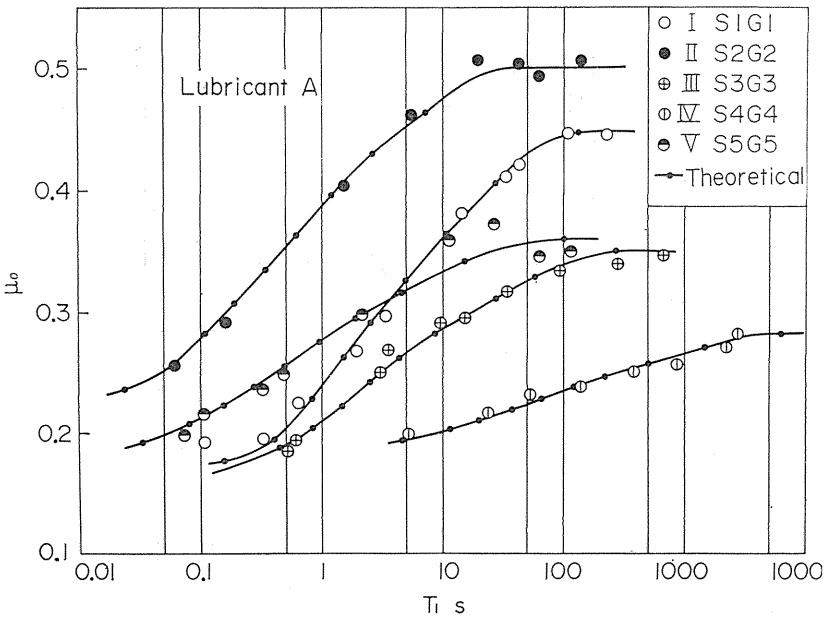

Fig. 91. Theoretical $\mu_0 - T_1$ curves for various surfaces.

applied lubricant is A. The values of parameters used in the calculation are summarized in Table 12.

Table 12. Calculation chart of Parameters

Surfaces	μ_s	μ_d	$\xi_1\xi_2$	$h_e \times 10^{-3}$ mm	Q mm^4
S1G1	0.450	0.156	1140	0.851	28.4
S2G2	0.500	0.213	480	0.950	3.1
S3G3	0.350	0.157	26500	0.280	1.27
S4G4	0.146	0.071	17900	0.467	90.9
S5G5	0.303	0.179	2270	0.736	6.0

Figure 92 shows the relation between Q, h_e, and $\xi_1\xi_2$ obtained from Fig. 91 and Table 12. It is seen in the figure that both Q and h_e are strongly affected by $\xi_1\xi_2$, Q increases and h_e decreases as $\xi_1\xi_2$ increases. The value of ξ is correlated

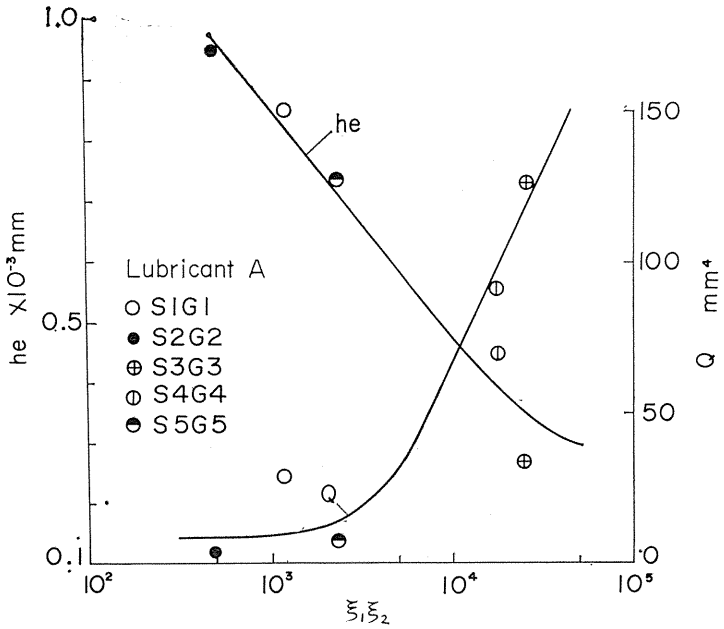

Fig. 92. Relation between Q, h_e, and ξ_1 ξ_2 for various surfaces.

with the so-called smoothness of the surface (ξ is large for smooth surface), and Q depends on the topography and the size of contact surface. If the surface is ideally smooth ($\xi\to\infty$), the value of Q is large and depends only on the size of the contact surface. Hence it is considered that Q increases as ξ increases. Initial effective film thickness h_e is approximated to the sum of the maximum deformation a_s and the adsorbed thickness of lubricant film h_e. And he depends primarily on a_s in general as described in the foregoing. The surface having a greater value of ξ gives a smaller value of a_s. Hence h_e decreases as ξ increases.

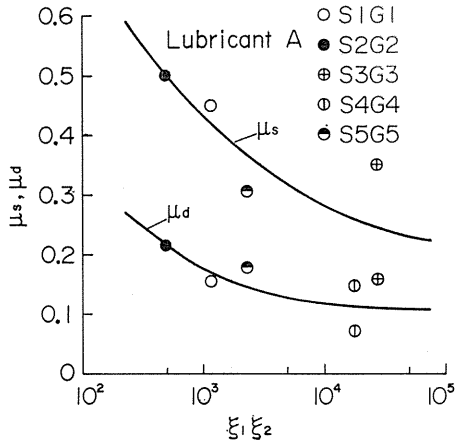

Fig. 93. Experimental μ_s, μ_d—$\xi_1\xi_2$ curves for various surfaces.

Figure 93 shows the experimental μ_s, μ_d versus $\xi_1\xi_2$ curves. It is recognized in the figure that μ_s, μ_d decreases with increasing $\xi_1\xi_2$ as predicted from the results shown in Figs. 85-88.

Figure 94 shows the theoretical $\mu_0 \sim T_1$ curves as a function of $\xi_1\xi_1$ calculated from the results shown in Figs. 92 and 93. In the calculation, the values of Q, h_e, μ_s, and μ_d are determined as follows; for $\xi_1\xi_2=500$, $Q=1.4\text{mm}^4$, $h_e=0.97\times10^{-3}$mm, $\mu_s=0.495$, $\mu_d=0.215$; for $\xi_1\xi_2=5000$, $Q=54\,\text{mm}^4$, $h_e=0.58\times10^{-3}$mm, $\mu_s=0.320$, $\mu_d=0.125$; and for $\xi_1\xi_2=50000$, $Q=140\,\text{mm}^4$, $h_e=0.28\times10^{-3}$mm, $\mu_s=0.522$, $\mu_d=$

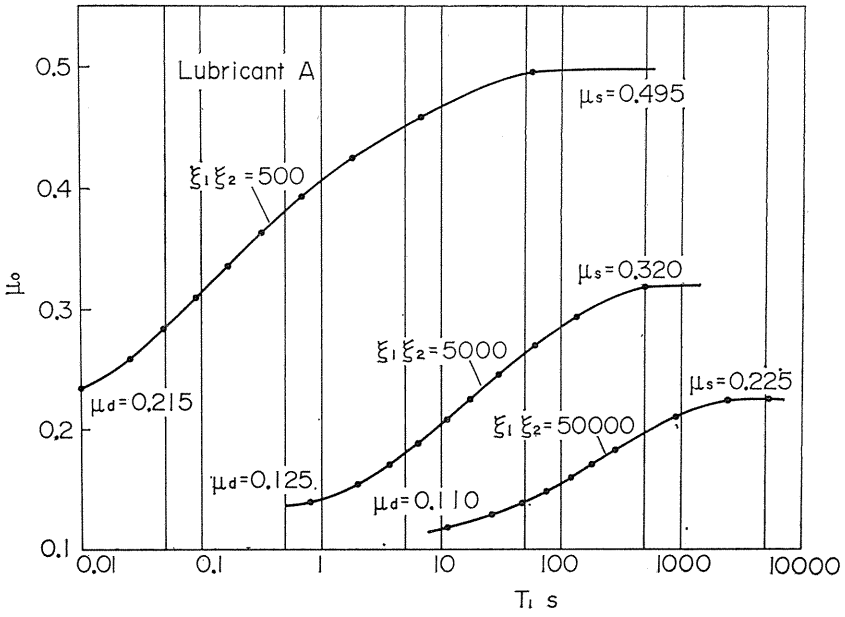

Fig. 94. Theoretical $\mu_0 - T_1$ curves as function ξ_1 ξ_2.

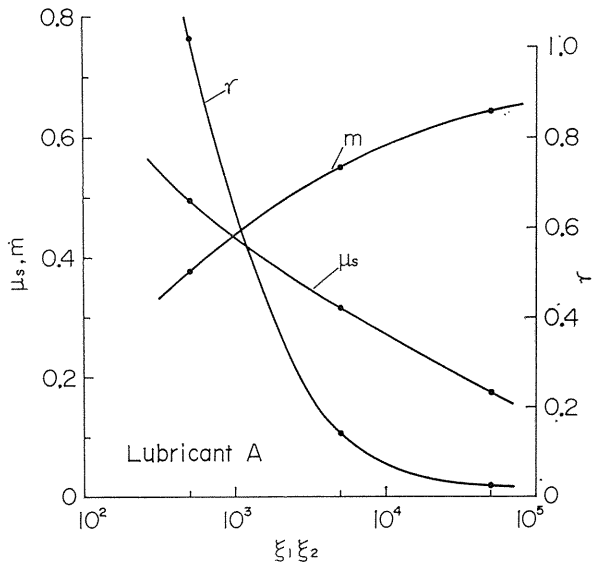

Fig. 95. μ_s, γ, and m versus ξ_1 ξ_2 curves.

0.110. It is seen in the figure that μ_s decreases as $\xi_1\xi_2$ increases, and the stick time required for μ_0 to approach the asymptotic value μ_s increases as $\xi_1\xi_2$ increases.

Figure 95 shows the relation μ_s, γ, m, and $\xi_1\xi_2$ obtained by applying equation (1) in the same way as described in the previous section. It is seen in the figure that μ_s, γ, and m depend strongly on $\xi_1\xi_2$, and that, as $\xi_1\xi_2$ increases, μ_s and γ decreases; it is especially notable that γ decreases abruptly and approaches 0, and m increases. The value of m depends but slightly on the properties of the lubricants as seen in Figs. 82 and 84 but rather considerably on the surface topography as seen in Fig. 95.

The results are that the effect of surface topography on the characteristics of static friction can be discussed theoretically using the new parameter, coefficient of surface topography ξ. It is considered that the frictional behaviour for any surface combination can also be examined in the same way.

Finally, some fundamental considerations on prevention of stick-slip motion are set forth on the basis of the results described in the foregoing.

The characteristics of stick-slip motion on a machine tool slideway depend markedly on both kinetic and static frictional behaviour especially the latter. If frictional behaviour can be estimated clearly, the characteristics of stick-slip motion can be approximately predicted.

The characteristics of its amplitude of stick-slip motion are most important. Amplitude a is relatively large and nearly constant in the range of low driving speed v and decreases abruptly as v increases, and in the range above a critical speed, a takes on a very small value, or stick-slip motion disappears. These behaviour can be qualitatively examined by the characteristics of static friction, namely the amplitude has a large value for a large static friction μ_0 and the critical spped is low as the stick time required for μ_0 to approach the asymptotic value is long. The characteristics of static friction are discussed from these points of view.

It is presumed from the results shown in Figs. 81 and 82 that, as the adsorbed lubricant film is thick, the values of μ_s and γ become small, and as a result, the amplitude becomes small and the critical speed decreases. In reference to Figs. 83 and 84, the value of γ decreases as the viscosity of lubricant increases, and as a result the critical speed decreases. In reference in Figs. 94 and 95, the surface having a large value of ξ takes small values of μ_s and γ, the amplitude becomes small and also the critical speed lowers.

Summarily speaking, in order to prevent the stick-slip motion, conditions are desirable where the values of μ_s and γ are small and the values of m and ξ are large.

7. 5. *Conclusion*

The mechanism of contact between sliding surfaces and load carrying mechanism under boundary lubrication are discussed. As a result, the mechanism of the time-dependence of static friction has been explained by the microscopic squeeze effect of lubricant produced by the relative approach of the contact surfaces.

The influence of properties of lubricant and surface topography on static friction is quantitatively investigated on the basis of an empirical formula. The results are that the viscosity of lubricants, the thickness of adsorbed lubricant

film which depends primarily on the chemical composition of lubricant, and the surface topography have a marked effect on the characteristics of static friction. The effects of surface topography on the characteristics of static friction are discussed theoretically with a new numerical parameter proposed to estimate the surface topography.

Based on the foregoing results, a general concept to prevent the stick-slip motion in machine tool slideways is advanced.

References

1) F. P. Bowden and D. Tabor, "The Friction and Lubrication of Solids" Clarendon Press, 1958.
2) E. Rabinowicz, "The Intrinsic Variables Affecting the Stick-Slip Process", Proc. Phys. Soc. London, Vol **71**, 1958.
3) J. B. Sampson, et al., "Studies in Lubrication", Jour. App. Phys., Vol. **14**, 1943, p. 689.
4) A. Matsuzaki, "Theoretical Analysis of Critical Conditions of Stick-Slip in Hydraulic Driving Mechanism", Japan Soc. Mech. Engrs. Vol. **29**, No. 206, 1963, p. 1615.
5) C. A. Brockley, et al., "Friction-Induced Vibration", Trans. ASME. Ser. F, Vol. **89**, No. 1, 1967, pp. 101-108.
6) B. R. Singh, "Stick-Slip Sliding under Forced Vibration" Jour. Science and Engng. Research" (India), Part II, Vol. **2**, 1958, pp. 227-232.
7) P. G. Howe et al., "London-Van der Waals Atractive Forces between Glass Surfaces", Canadian Jour. Chem. Vol. **33**, No. 9, p. 1375-1383.
8) B. V. Derjaguin et al., "A Theory of Stick-Slip Sliding of Solids", Proc. Conference on Lubrication and Wear, London, Oct. 1957, p. 257-268.
9) E. Rabinowicz, "Friction and Wear of Materials", Wiley, N. Y., 1955, p. 60.
10) K. Okamura et al., "Study on Frictional Vibration", Jour. Japan Soc. of Precision Engng., Vol. **34**, No. 11, 1968, p. 33-36.
11) F. Hensen, Indust. Anzeiger, Jg. 16, Nr. 12, 1960, S. 575.
12) M. Mitsui, Jour. Mech. Lab., Vol. **19**, 1965, p. 1.
13) K. Okamura et al., "Study on Frictional Vibration", Jour. Japan Soc. of Precision Engng., Vol. **34**, No. 12,1968, p. 774-779.
14) S. Shiozaki et al., Trans. Japan Soc. Mech. Engrs., Vol. **35**, No. 269, 1969, p. 211.
15) J. F. Archard, "Contact and Rubbing of Flat Surfaces", Jour. Appl. Phys. Vol. **24**, No. 8, 1953, p. 982.
16) I. V. Kraghelsky, "Friction and Wear", 1965, Butterworths.